universität wien

MASTERARBEIT / MASTER'S THESIS

Titel der Masterarbeit / Title of the Master's Thesis

„Transcriptomic and Immunohistochemical Analysis of T cell activity in PCD model L7-HA"

verfasst von / submitted by

Anja Steinmaurer

angestrebter akademischer Grad / in partial fulfilment of the requirements for the degree of

Master of Science (MSc)

Wien, 2020/ Vienna, 2020

Studienkennzahl lt. Studienblatt / degree programme code as it appears on the student record sheet:	UA 066 834
Studienrichtung lt. Studienblatt / degree programme as it appears on the student record sheet:	Masterstudium Molekulare Biologie
Betreut von / Supervisor:	Ao.Univ.Prof. Dr. Jan Bauer

Table of Contents

Acknowledgement

I would first like to express my deepest gratitude to my thesis advisor Prof. Dr. Jan Bauer of the Neuroimmunology department at the Center of Brain Research to give me the opportunity to work with him on this project. He provided insightful comments and I truly appreciated the feedback and the great support offered by him. It was a big pleasure to work with him.

I also owe a very important dept to Anna Tröscher, PhD, who has been an extraordinarily tolerant and generous teacher to me. The door of her office was always open when I ran into a trouble spot or had some questions about my research or writing. I really appreciate her as a person and colleague.

I have also greatly benefited from the advice given by Ulrike Köck, MSc and Marianne Leißer who shared with me their excellent knowledge of histochemistry and provided technical assistance during my experiments.

My special thanks go to all my colleagues in the department, who not only enriched my working days but also my personal life. I will always keep my time here as a particularly positive memory.

Of course, my family and my boyfriend also made big contribution to the success of my work. They consistently supported and encouraged me to bring out the best of me which really helped me to stay patient and to stick to my goals.

1. Abstract

Paraneoplastic neurological degeneration is a severe disorder characterized by an extensive loss of Purkinje cells in the cerebellum which is accompanied by high mortality. In this disorder, patients suffer from a tumour which produces an oncoprotein that is simultaneously expressed in the cerebellum. The immune system recognizes the antigens and induces a response resulting in cerebellar tissue damage predominantely caused by the cytotoxicity of CD8+ T cells. During cerebellar inflammation, activated CD8+ T cells have been detected in close proximity to Purkinje cells and found to produce harmful amounts of IFN-γ which further promotes inflammation. [1] Since, the introduction of immune checkpoint inhibitors (ICIs), PCD has gained increasing attention. ICIs aim to elicit an effective immune response against the tumour, however, they also inhibit the control mechanisms that prevent an overreaction of the immune system. In rare cases, the application of ICIs is accompanied by paraneoplastic syndromes, including PCD. Due to the severe neurological symptoms, immunological events, especially the role of IFN-γ and its potential as a therapeutic target, have to be further investigated[2,3]

In this project L7-HA mouse model exhibiting the pathology of PCD was used to investigate T cell activity and its correlation with IFN-γ presence. The focus was put on the effect of anti-IFN-γ antibodies which aimed to neutralize IFN-γ in the peripheral tissue of this mouse-model.[1] Different groups of this mouse model received distinct treatments. Upon sacrifice of the subjects, transcriptomics were used to perform a comparative analysis of pathways differentially expressed in the cerebellum of the distinct groups. Moreover, immunohistochemical detection of T cell numbers and pSTAT-positive cells helped to validate the results. In addition, confocal microscopy was used to analyse the presence of pSTAT1, MHC class I and calbindin positive cells in the cerebellum of the differently treated animals.

Results revealed that anti-IFN-γ treated animals show an upregulation of pathways involved in neuronal homeostasis compared to untreated animals with PCD pathology. Untreated animals showed an upregulation of proinflammatory pathways involved in functions, such as IFN-γ response and exhibited high numbers of T cells and pSTAT1-positive cells in the cerebellum. Confocal microscopy further confirmed these findings.

Anti-IFN-γ treated animals mostly showed absence or only slight increase of MHC class I molecules on cell surface and calbindin levels were closer to physiological conditions compared to untreated animals. These findings further confirm the great potential of anti-IFN-γ antibody as useful anti-inflammatory therapy against PCD.

2. Zusammenfassung

Paraneoplastische neurologische Degeneration ist eine schwere Erkrankung begleitet von massivem Verlust von Purkinje-Neuronen und einer hohen Sterblichkeit. Patienten mit dieser Krankheit leiden an einem Tumor, welcher Antigene produziert, die gleichzeitig im Cerebellum exprimiert werden. Das Immunsystem erkennt diese Antigene und induziert eine Immunantwort, welche zur Schädigung des cerebellaren Gewebes führt. Diese Schädigung wird vorwiegend durch zytotoxische DC8+ T-Zellen verursacht. Während dieser cerebellaren Entzündung konnten aktivierte CD8+ T-Zellen in der Nähe von Purkinje-Zellen detektiert werden, wobei diese schädliche Mengen IFN-γ produzierten. IFN-γ förderte widerum die Entzündungskaskade. Mit der Einführung von Immuncheckpoint-Inhibitoren (ICIs), erlangte PCD wieder mehr Aufmerksamkeit. ICIs streben grundsätzlich eine effektive Immunantwort gegen den Tumor an, allerdings inhibieren sie auch wichtige Kontrollmechanismen, welche normalerweise eine Überreaktion des Immunsystems verhindern. In seltenen Fällen, treten durch die Anwendung von ICIs paraneoplastische Symptome aus, wie zum Beispiel PCD. Auf Grund der schwerewiegenden neurologischen Symptome, ist es von großer Bedeutung, die immunologischen Mechanismen, insbesondere die Rolle von IFN-γ sowie sein Potenzial als therapeutisches Zielmolekül, weiter zu erforschen.

In diesem Projekt wurde das Mausmodell L7-HA mit PCD-Pathologie verwendet, um die T-Zell-Aktivität, sowie deren Korrelation mit der Präsenz von IFN-γ untersucht. Dabei wurde der Fokus auf den Effekt von Anti-IFNγ-Antikörpern, welche IFN-γ im peripheren Gewebe des Mausmodells. neutralisieren sollten, gelegt. Verschieden Gruppen des Mausmodells erhielten verschiedene Behandlungen. Post mortem wurde mit dem cerebellaren Gewebe der Tiere eine transkriptomische Analyse durchgeführt, um Genexpressionswege der Cerebella der verschiedenen Behandlungsgruppen zu vergleichen. Des Weiteren wurden T-Zellen und pSTAT-positive Zellen quantifiziert, um

die transkriptomischen Resultate zu bestätigen. Die konfokale Mikroskopie wurde verwendet, um Korrelationen zwischen pSTAT1-, MHCI- und Calbindin-positiven Zellen in den verschiedenen Behandlungsgruppen zu analysieren.

Die Resultate ergaben, dass Anti-IFN-γ-behandelte Tiere im Vergleich zu unbehandelten Tieren eine Aufregulierung von Genexpressionswegen, welche an der neuronalen Homöostase beteiligt sind, zeigen. Unbehandelte Tiere wiesen eine Aufregulierung von inflammatorischen Genexpressionswegen auf. Diese waren in Funktionen, wie die IFN-γ-Antwort, involviert und zeigten eine hohe T-Zell- und pSTAT1-positive Zell-Zahl im Cerebellum. Bilder der konfokalen Mikroskopie unterstützen diese Beobachtungen. Anti-IFN-γ-behandelte Tiere wiesen meistens eine Abwesenheit oder minimale Erhöhung von MHC-I-Molekülen an der Zelloberfläche auf. Die Menge an Calbindin war in diesen Tieren näher an physiologischen Niveaus, verglichen zu unbehandelten Tieren. Diese Beobachtungen bestätigen das große Potenzial des Anti-IFN-γ-Antikörpers als mögliche anti-inflammatorische Therapie gegen PCD.

3. Introduction

Paraneoplastic neurological syndromes (PNS) involve a range of disorders of the nervous system associated with the presence of cancer and show a rare occurrence of less than 1/10.000 of cancer patients. Normally, the immune system regards cancer cells as foreign and initiates immunological responses to fight the tumour. In PNSs, the immune system targets distinct proteins, expressed on the tumour but also in the nervous system, so called onconeural antigens. This immune reaction can lead to severe damage of the peripheral (nerves, neuro-muscular junction) as well as the central nervous tissue (brain, spinal cord).[4,5] In recent years, the establishment of immune-checkpoint inhibitors (ICI) in cancer treatment has drawn further attention to clinical relevance of PNSs. Immune checkpoints (ICs) are receptor molecules located on immune cells, i.e. T cells, and build essential components in preventing an overactivation of the immune response, which could lead to auto-immune reactions. Tumours can “hijack” these immune checkpoints to dampen the anti-tumoral immune response. Therefore, immune-checkpoint inhibitors (ICIs) have been established in anti-cancer therapy to restore effective immune response against malignancy. However, the immune-activating effect of ICIs is related to an

increased risk of cell-mediated and humoral immune responses directed against self-antigens resulting in a variety of paraneoplastic neurological syndromes, such as paraneoplastic cerebellar degeneration (PCD).[6] PCD is a distinct subtype of PNSs and is characterized by tumour-related autoimmune responses directed against antigens in the cerebellum.[7] A recent study deals with Yo-antibody mediated PCD in a mouse model and demonstrates $CD8^+$-T cells and the cytokine IFN-γ to play striking roles in the pathology of PCD. Treatment with anti-IFN-γ antibody lead to neutralization of INF-γ and increased protection from PCD symptoms in mice.[1] However, the anti-tumoral immune response remained effective. Hence, the immunological events in PCD, especially under the condition of ICI and anti-IFN-γ antibody treatment, require further investigation for a better understanding of the pathology of PCD.

3.2. Inflammation in the CNS

Inflammation is a natural defence mechanism to harmful events, e.g., injury or infection. The main function of inflammation is to fight and clear the detrimental stimuli causing cell damage. Therefore, the host initiates a cascade of immunological events to maintain homeostasis of the tissue. This process involves responses of the non-specific, innate and the specific and acquired adaptive, immune system.[8,9] An interplay of specific components, e.g., the blood brain barrier (BBB), astrocytes, microglia and peripheral immune cells as well as cytokine secretion, constitute the basis of the inflammatory response in the CNS. [10,11] Neuroinflammation is defined as immune-mediated inflammatory response occurring in the central nervous system (CNS). Until a few years ago, the CNS was considered to be “immune privileged” and regarded as immunologically isolated from the peripheral immune system via the blood brain barrier (BBB). In the 20th century, the term “immune privileged” referred to the brain being incapable of initiating or promoting immune responses on its own. Hence, the immune privilege (IP) of the CNS was assumed as neural defence mechanism to prevent detrimental inflammation of the brain [10,12,13] However, extensive research in the field of neuroimmunology has redefined this conception of immune privilege. Nowadays, it is well known that BBB is a semipermeable network that enables a crosstalk between the central and the peripheral immune system. Aside from engaging in preservation of brain homeostasis, circulating immune cells, e.g. surveilling T cells, have been observed to engage in immune reactions

in the CNS. Especially under inflammatory conditions, the BBB exhibits a certain extend of leakiness that allows antibodies, peripheral immune cells, inflammatory mediators ,e.g. cytokines, to overcome the BBB and reach the brain parenchyma, thus, eliciting inflammation which eventually results in cell and tissue damage.[14–16] A short-lasting inflammation in the CNS, e.g. involving microbial invasion or trauma in the CNS, is regarded as beneficial and protective whereas persistent neuroinflammation is related to several neurological disorders. Hence, immunological mechanisms in CNS inflammation and its resulting pathology have gained increasing attention over the last decades.[17]

3.3. Innate Immunity

The innate immune system is the non-specific, first-responding part of the immune system that reacts rapidly to foreign organisms and harmful tissue damage. From birth on, players of the innate immunity monitor all organs and body tissues, prepared to fight invading pathogens. In contrast to adaptive immunity, the innate immune system does not retain memory after counteracting intruders. The innate immune system is composed of physical barriers, cellular components, specific recognition receptors and soluble mediators; e.g., Cytokines and complement system. Physical barriers of the innate immune system aim to build chemical and structural obstructions to prevent invasion of foreign organisms. They include skin, epithelial and mucous membranes. If pathogens are still capable of invading the host, a cascade of responses involving phagocytes, i.e. macrophages and dendritic cells (DCs), natural killer cells and the complement system, are elicited. [18–21]The central process of innate pathogen elimination includes the mechanism of phagocytosis. Importantly, phagocytic cells are activated via binding to opsonins, phagocytosis-enhancing molecules on the surface of pathogens. Phagocytes, amongst other cell types, also can sense harmful objects via distinct pattern recognition receptors (PRR), e.g. Toll-like receptors (TLRs) or scavenger receptors. PRRs are located either on the surface of phagocytes or intracellularly and are bound by pathogen-associated molecular patterns (PAMPS) derived from foreign organisms, or damage-associated molecular patterns (DAMPs). DAMPS origin from the host and act as warning signals resulting from tissue damage. Upon this process of recognition, phagocytes

internalize the foreign particle and enclose it within a vesicle, i.e. phagosome, decompose it and present particles of the metabolize.[22,23]

3.3.1. Innate Immunity in the CNS

Considering the cells of innate immunity of the central nervous system, glial cells play a central role in pathogen and tissue damage elimination as well as in T cell activation. Glia constitute 90% of the cells in the CNS and comprise microglia, astrocytes, ependymal cells and oligodendrocytes. [24,25]

Microglia

Microglia act as the primary resident macrophages in the CNS and constitute 10-15% of all cells in the CNS of mammals. They are located in brain parenchyma, spinal cord, retina, optic nerve and originally derive from the yolk sac. In a resting state, microglial cells fulfil essential homeostatic functions which means that they permanently monitor their environment for disturbances, e.g. pathogens or cell damage, and directly interact with neurons, astrocytes and blood vessels. This allows them to adapt quickly and dynamically to variable conditions in the CNS. Non-activated microglial cells exhibit a highly branched morphology and a small nucleus and, therefore, differ from macrophages and dendritic cells (DCs). [17,26–29]When microglia are activated due to pathologic changes, their shape changes to an amoeboid state and their branches diminish in size. They effectively phagocytose intruders as well as necrotic cells. Microglia also secret various chemokines, thus, attracting more immune cells to the disrupted area. Moreover, production of microglial growth factors and anti-inflammatory substances are essential for neuronal tissue damage repair. [25,30]

Astrocytes

Astrocytes are the most prevalent glia subtype of the CNS and make up a proportion of 20-40% of all brain cells.[31] Due to distinct morphological features and locations, astrocytes are mainly subdivided into protoplasmic (located in grey matter) and fibrous (found in white matter) astrocytes. For the pathology of PCD, a relevant specialized astrocytic cell type is the Bergmann glial cell, which is located in the Purkinje cell layer of the cerebellar cortex. It exhibits very long extensions leading through the molecular layer.[32] The typical shape of an astrocyte reminds of a star displaying numerous dendritic

cell protuberances. The branches of protoplasmic astrocytes are normally too dense to be differentiated whereas the separate processes of fibrous astrocytes are clearly visible. [33] Formerly, the function of astrocytes was classically assumed to participate in scaffolding neurons. However, astrocytes have been revealed to be important players during brain development and tissue homeostasis, too.[34,35]In detail, they regulate ion and water transport, maintain proper pH levels, support neural nutrient supply and participate in synapse pruning. They also form essential parts of the blood brain barrier (BBB) as well as the blood-cerebrospinal fluid barrier (BCSFB). In case of infection, CNS inflammation or tissue damage, astrocytes secret various pro-inflammatory mediators such as chemokines and cytokines. In contrast, they produce anti-inflammatory cytokines and contribute to neuroprotection during degenerative and remyelinating processes. Therefore, astrocytes perform essential tasks maintaining structural and functional stability of the CNS. [34]

The Blood Brain Barrier

The brain´s most essential first line of defence is the blood-brain barrier (BBB). To ensure brain homeostasis, a complex physiological system of microvessels forms a connection between the peripheral blood circulation and the CNS. On the one hand, this unique anatomical structure, referred to as “Blood-Brain Barrier”, allows the supply of neural tissue with oxygen and nutrients and on the other hand also carries out an essential immunological function that shields the CNS from pathogens and toxins. Therefore, the BBB represents a structural and biochemical barrier. The anatomy of the BBB comprises an endothelial cell (EC) layer, a basement membrane, pericytes and astrocytic endfeet. Endothelial cells build up the vascular walls of the BBB, are held together by tight junction proteins and are not fenestrated as seen in other tissues. The expression of specific transporter allows them to tightly regulate the transport of molecules and cells between the brain and

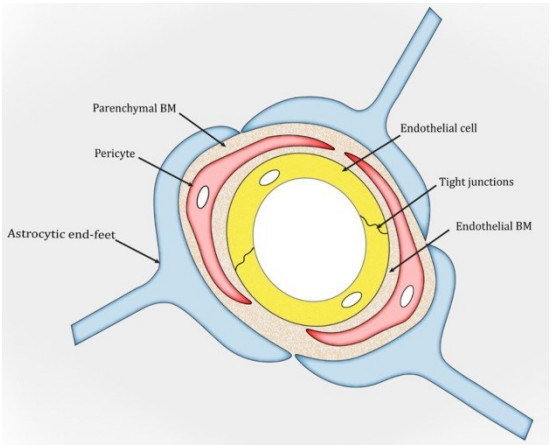

Figure 1 Structure of the Blood brain Barrier

Astrocytic endfeet are shown in blue. Endothelial and parenchymal basement membrane are shown in beige. Pericytes are demonstrated in red. Endothelial cell is shown in yellow (Xu et. al; 2019).

the periphery.[36] The basement membrane (BM) is subdivided into parenchymal and endothelial BM surrounding the pericytes. The BM delivers structural stability and supports cell anchoring.[37] Pericytes function as contractile cells on the blood vessels for blood flow regulation, passaging of immune cells and general homeostasis of the BBB.[38] Astrocytic endfeet further form a barrier between brain and peripheral blood vessels (Figure 1). They ensheathe the CNS vessels and contribute formation of the BBB. Astrocytic endfeet also participate in blood flow regulation, i.e. dilation and constriction of vessels, and maintenance of EC properties. [39,40]The so-called Virchow-Robin space is located between EC and brain tissue and contains macrophages. The complex of the BBB where neurons, astrocytes, microglia and components of the BBB interact is called neurovascular unit (NVU). [41,42]

While the BBB guarantees brain homeostasis in healthy individuals by restricting the exchange of cells and molecules between brain tissue and periphery, the structure and functionality of the BBB can be severely disrupted under inflammatory conditions. Break-down of the BBB through systemic inflammation allows cells and pathogens to invade brain parenchyma. The disrupted BBB can be accompanied by histological changes involving damage of endothelial cells or tight junctions, but also changes on a molecular level including for example upregulation of EC receptors and changes in astrocyte activity (Figure 2). As a consequence, the immune cells, inflammatory molecules and antibodies can cross the BBB and invade the brain parenchyma and lead to neurodegeneration. [43]

3.4. Adaptive Immunity

The adaptive immune system forms the second line of defence and becomes active if pathogens or cell damage cannot be contained by innate immune responses. In contrast to innate immunity, components of adaptive immunity react slower and highly specific to environmental changes. An essential function of adaptive immune response is to distinguish between self and foreign antigens to prevent autoimmune reactions against

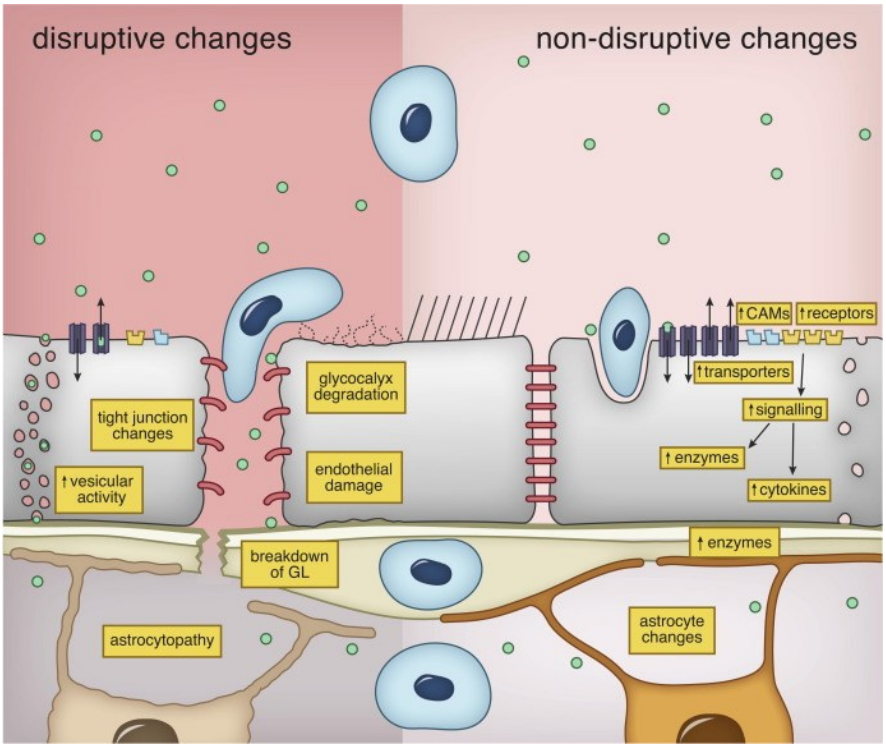

Figure 2 Disruptive and non-disruptive changes in the BBB

Breakdown of the BBB can involve changes involving physical damage or molecular changes. Physical damage is also regarded as disruptive alteration and iis characterized by a change in anatomy. Molecular changes are described as non-disruptive and usually does result in functional disturbances, predominantely in cell trafficking (Varatharaj, Galea; 2017)

endogenous tissues. The main mediators of adaptive immunity are white blood cells, also called lymphocytes. They are subdivided into B- and T cells and play a central role in two different types of adaptive immune responses involving antibody (humoral) responses and cell-mediated immune responses. For antibody responses, B cells transform into plasma cells which secret immunoglobulins. Antibodies are located in the blood as well as in extracellular fluids and can circulate through the body. They have the ability to bind antigens specifically and to inactivate the intruder. This process is called “neutralization”.

A further function of antibodies is to mark bacteria and viruses by encasing them. This "opsonisation" by antibodies helps phagocytes to detect pathogens and metabolize them. Furthermore, antibodies also activate the complement system which involves different plasma proteins which also contribute to recognition and destruction of pathogens. The five main classes of antibodies include IgA, IgD, IgE, IgG and IgM. Each of them fulfils different functions and reacts to distinct antigens.[44,45]

The central players of cell-mediated immune responses are T lymphocytes. They are produced in the bone marrow and mature in the thymus. T cells which have never bound to antigens are termed as "naïve" T cells.[46] In order to initiate an effective immune response, naïve T cells have to get activated by antigen-presenting cells (APCs), e.g. dendritic cells, B cells, fibroblasts. An essential component of antigen presentation process is a specific protein complex, called major histocompatibility complex (MHC). MHCs are classified into MHC class I and class II molecules and are located on the surface of distinct cells types. MHC class I molecules are located on nucleated cells and present intracellular peptides produced in the cytosol, e.g., viral peptides. MHC class II molecules are restricted to the surface of only certain cell types, such as macrophages, DCs and B cells. They present extracellular antigens to naïve T lymphocytes, e.g., viral particles metabolized and presented by phagocytes. There are different subtypes of naïve T cells specified by different co-receptors. Helper T cells express the CD4 co-receptor which specifically binds to MHC class II molecules. Cytotoxic T cells display the CD8 co-receptor on their surface which binds to MHC class I molecules. T cells circulate through the blood and lymphatic system of the body and are usually activated in the lymph nodes where the antigens are presented to T cells. For antigen recognition, T cells own a great variability in T cell receptors (TCRs) which can bind to distinct antigens. When the T cell recognizes an antigen on the surface of an APC, it binds the foreign peptide with its TCR. Consequently, the T cell is activated, initiates cytokine secretion and differentiates into a mature or effector T cell. Activated CD8+ T cells start to proliferate and mainly function as destroyers of infected cells and cancer cells. Furthermore, they produce different cytokines promoting inflammation, whereby IFN-γ is one of the most characteristic cytokines. After clearance of the pathogen, some effector cells remain as memory T cells which enables a more effective response in case of repeated infection with the same

pathogen. Naïve CD4 T + cells can transform into different subtypes upon their activation. The distinct subtypes, i.e., T-helper 1 cells (Th1), T-helper 2 cells (Th2), T-helper 17 cells, (Th17) and regulatory T cell, display characteristic cytokine profiles, including IL-4, IL-5, IL-9, IL-13, IL-10 and IL-15. CD4+ T cells show a great variability in their tasks and mainly regulate the extent of the immune response and the establishment of memory T cells but also participate in direct cytotoxicity against pathogens.[44,47–49]

3.5. Cancer

3.5.1. Development of Cancer

Cancer can result from functional and structural dysfunctions of the organism including accumulation of mutations and altered signal transduction. These changes mainly affect genes responsible for cell division.[50] In a healthy organism, the proportion between cell division and cell death is strictly regulated by a complex system of cellular circuits.[51] In the course of cell division, the cell has to pass several checkpoints to control its functionality and proper cell growth. These control mechanisms also determine if the cell is stable enough for further differentiation steps or if it has to be eliminated through programmed cell death (apoptosis).[52] A disruption in one of these processes may lead to the production of deficient cells characterized by uncontrolled growth and proliferation, hence, resulting in tumour initiation.

The development of cancer can be divided into following steps; initiation, tumour promotion and progression. The initiation phase is characterized by the erroneous production of a malignant cell based on the influence of carcinogenic factors[53], e.g., physical inactivity, tobacco, alcohol use or infections[54]. In the promotion phase, cell clones with enhanced growth rates and new genetic properties drive tumour progression and inhibition of tumour suppressor genes. In the progression phase, the tumour grows and can develop metastases in case of malignancy (Figure 3). [55]

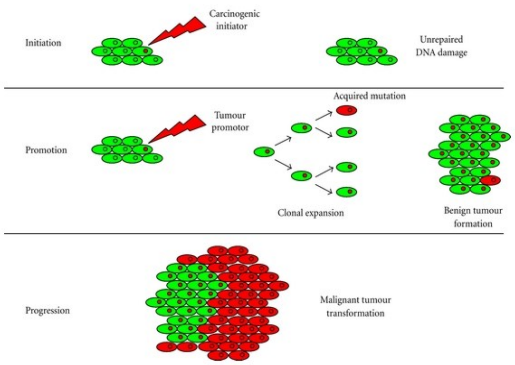

Figure 3 Three-step Model of Cancer Development

Development of cancer is often elicited by a fail of DNA repair mechanisms that lead to an accumulation of mutations. Tumour can promote their growth and inhibit tumour suppressor genes. The main goal of the tumour is to metastasize and ensure its nutrition supply by generating own vasculature (Centelles; 2012).

3.5.2. Cancer Immunoediting

The immune system permanently surveys the human organism for potential pathogens and noxious substances and therefore has to differ between "self" and "non-self" tissue.[56] Due to their altered genetic constitution, cancer cells express genes which encode for proteins, called tumour antigens. The immune system recognizes tumour antigens on the surface of cancer cells as "foreign" and can initiate immune responses to eliminate them.[57] Despite of that, cancer cells aim to promote their expansion and, therefore, occupy properties that enable them to stay hidden from immune surveillance.

Recently, the model of cancer immunoediting has been established and states a dual role of the immune system that can participate in both host protection from malignancy but also providing a microenvironment for tumour cells and therefore contributing to tumour progression. Three steps are involved into the concept of immunoediting. The process of elimination describes the control and elimination of cancer cells through host immune responses. [58] When a tumour has reached a distinct size, it starts to grow its own blood vessels through the process of angiogenesis to provide proper oxygen and nutrient supply for its further progression. [59] In this phase the tumour starts to produce angiogenic proteins and grows invasively into the host tissue which causes damage of host tissue (Figure 4). This elicits immune responses involving APCs that present tumour proteins via

MHC class I molecules to CD8+ T cells, natural killer cells and dendritic cells (DCs). Furthermore, phagocytes cross-present further antigens to CD8+ T cells, CD4+ T cells, natural killer cells and also B cells. Effector T cells then produce IFN-γ, which induces apoptosis and has a growth-inhibiting effect on the tumour. IFN-γ also promotes the release of chemokines, which also contributes to cancer cell death and suppression of angiogenesis. At best, all tumour cells can be fully eliminated by cytotoxic T cells and complete tumour regression is achieved. [58,60]

In case of PNSs an autoimmune reaction is related to anti-tumour immune responses. As already mentioned, cancer cells own specific proteins on their surface which can be recognized by the immune system. In the case of PNS, proteins normally restricted to the nervous system are expressed in both, tumour and nervous tissue. These proteins are called “onconeural antigens” and elicit immune responses directed against the tumour and, hence, also healthy nervous tissue gets attacked.[2] In detail, the tumour expresses onconeural antigens recognized by innate immune cells which consequently attack the tumour. This leads to release of tumour antigens. APCs are then able to pick up these antigens, travel to the lymph nodes and present the antigens to naïve CD4+ T cells via MHC class II molecules. CD4+ T cells start to expand and transform into CD4+ helper cells. They activate B cells which differentiate into plasma cells and start to produce antigen-specific antibodies. APCs also cross-present tumour antigens via MHC class I molecules to naive T cells that consequently differentiate into CD8+ cytotoxic effector T cells (CTLs). Subsequently, onconeural antigen-specific antibodies and T cells attack the tumour and the nervous tissue.

Cancer cells, that survive the immune response of elimination phase, enter a phase of “dormancy” in which the number of cancer cell eliminations and divisions is quite stable. Malignant cells use this period to improve their genetic constitution to pass into escape phase.[61] Cancer cells that could establish immunosuppressive mechanisms during equilibrium phase could enter the stage of immune escape. The tumour can now successfully outwit immune surveillance. Characteristic properties of tumour cells are downregulation of MHC class I and absence of co-stimulatory molecules essential for antigen presentation, production of immunosuppressive substances for inhibition of host immune responses or also modulation of other immune cells for promoting tumour

growth. Not later than in this critical stage the host requires clinical treatment against the tumour, else the probability of death would strikingly increase. [58,62]

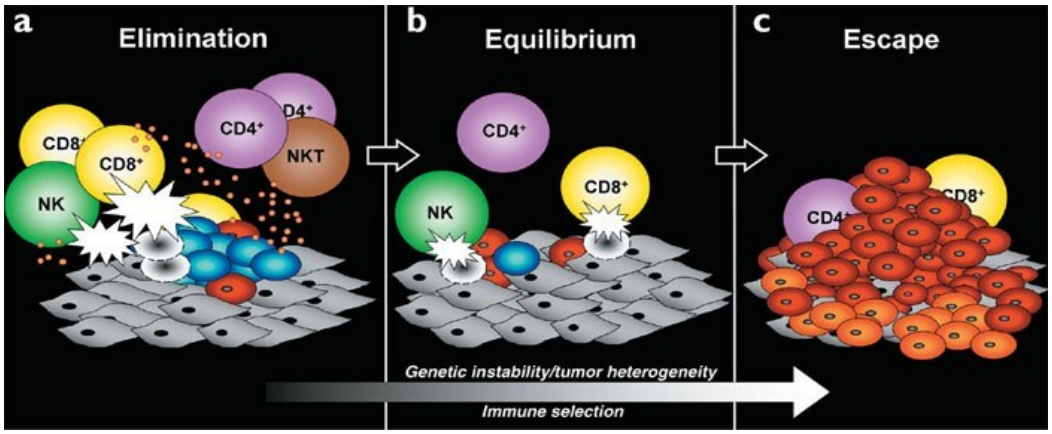

Figure 4 Stages of Immunoediting

The process of cancer immunoediting describes the tumour´s aim to establish in the organism´s body without being recognized by surveilling components of the immune system. The process is divided into three phases including elimination, equilibrium and escape phase (Dunn, et al.; 2002).

3.6. Immune checkpoints and their Inhibitors

Immune checkpoints (IC) are part of an immunological regulatory system that, in healthy individuals, prevents an overreaction of T cell responses to antigens and, hence, preserves self-tolerance. It keeps T cells from attacking healthy host tissue which could consequently result in autoimmune disease. IC receptor molecules are located on the surface of T cells and bind to distinct receptors on APCs or tumour cells in the course of T cell-activation. As a result, the extent of the immune response is regulated by the balance between co-stimulatory and inhibitory signals. Amongst others, prominent checkpoint molecules are Cytotoxic T Lymphocyte Antigen- 4 (CTLA-4) and Programmed Death-1 (PD-1) (Figure 5). [63,64]

3.6.1. CTLA-4

CTLA-4 is the most examined checkpoint receptor molecule and has inhibitory function. It is a homolog of the stimulatory co-receptor CD28. Both are transmembrane proteins and primarily expressed by T cells. CTLA-4 expression usually increases upon T cell activation and is decreased in naïve or resting T cells. The natural ligands of CTLA-4 and CD28 are B7-1 (CD80) and B7-2 (CD86) whereas CTLA-4 has a higher binding affinity for

B7 than CD28. The ligands CD80 and CD86 are located on APCs which are primarily found in lymph nodes.[65–67] CTLA-4 can compete with CD28 for binding the ligand B7. The binding of receptor CD28 results in a stimulatory signal which leads to IL-2 secretion and proliferation of T cells. In contrast, binding of CTLA-4 leads to decreased IL-2 secretion and reduced proliferation of T cells. The ratio of CD28 and CTLA-4 binding B7 designates whether T cells are activated or not.[68] Moreover, CTLA-4 is also found on regulatory T cells which in turn have an inhibitory effect on effector T cells and therefore also constitute to immunological tolerance[66,69,70]

3.6.2. PD-1

PD-1 is part of the B7/CD28 receptor family and also acts as inhibitory receptor. In contrast to CTLA-4, PD-1 is primarily located on T cells in tissues and tumours. PD-1 binds the ligands programmed death ligand 1 (PD-L1), also named B7-H1 or CD274, and programmed death ligand 2 (PD-L2), also referred to as B7-DC and CD273.[63] Whereas CTLA-4 ligands are primarily located on APCs, PD-1 ligands can be found on a greater variety of cell types. PD-L1 is located on leukocytes, non-hematopoietic cells, non-lymphoid tissues, parenchymal cells as well as tumour cells. PD-L2 is predominantly present on dendritic and monocytes. Ligand binding by PD-1 leads to suppression of T cell proliferation and IFN-γ production, but also decreased IL-2 production. As CTLA-4, PD-1 is also present on regulatory T cells and promotes their proliferation in order to control effector T cell activity. [71]

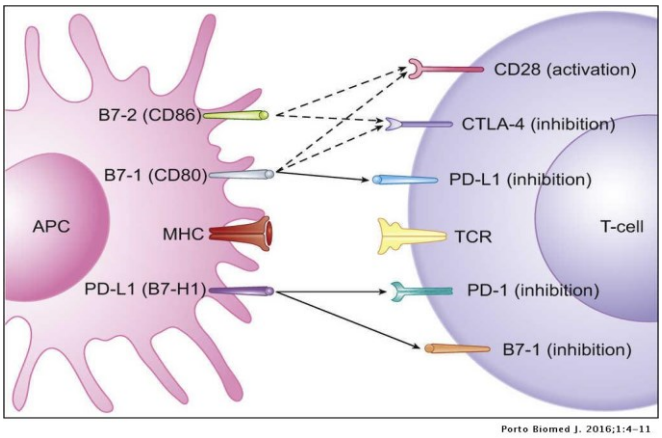

Figure 5 Inhibition of Immune checkpoints with ICIs

APCs provide surface ligands that bind to the checkpoint receptors. CTLA-4 and PD-1 account for the most commonly known inhibitory receptors. Each of them is found on distinct cell types and influences T cell activity. (Silva, Gullo, et.al, 2016)

3.6.3. Immune Checkpoint Inhibitors

As described above, immune checkpoints are fundamental in the regulation of T cell responses to avoid immune overreaction and inflammatory host tissue damage, possibly resulting in autoimmune-disease. Immune checkpoint inhibitors (ICI) aim to block the inhibitory checkpoint mechanisms by enabling an enhanced immune response. As cancer cells develop the ability to suppress host immune responses during tumour development, these checkpoint blockades have been established in anti-cancer therapy to achieve a more effective anti-tumour response.[72] The best examined ICIs are anti-CTLA-4 antibody and anti-PD-1 antibody which elicit prominent T cell responses against the tumour accompanied by increased IFN-γ production.[73,74]Both inhibitors show striking improvements in the overall and progression-free survival of patients suffering from different cancer types. Cancer types most successfully treated with ICIs include melanoma, renal cell carcinoma, Hodgkin´s lymphoma and non-small cell lung cancer. [75]

3.7. Paraneoplastic Neurological Syndromes

Although ICIs show beneficial effects in anti-cancer therapy, in rare cases their application is accompanied by so-called immune related adverse effects (irAEs) resulting from exaggerated immune reaction against healthy body tissues. IrAEs can arise in any organ and tissue and most commonly affect the gastrointestinal tract, skin, liver and endocrine system. A small proportion of patients also display neurological immune-related adverse events (nirAE), often manifesting as paraneoplastic neurological syndromes (PNSs). PNSs are in general difficult to diagnose due to their unspecific clinical picture and are accompanied by a high mortality rate.[2,76–79] PNSs can affect the central (brain) as well as the peripheral part (peripheral nerves) of the nervous system. The term “Paraneoplastic” refers to the fact that the pathologic symptoms are not elicited by the tumour itself, but by immune responses directed against the tumour. [80,81]

3.7.1. Antibodies in PNS

Antibodies targeting onconeural antigens are essential markers in PNS diagnosis and are usually detectable in the serum and cerebrospinal fluid (CSF) of PNS patients. Antibodies contribute to the pathogenicity of PNS depending on their location. In PNS, antibodies targeting proteins on the cell surface can be present with or without an underlying tumour. Due to its superficial location, the antigen is accessible for the antibody´s pathogenic effect. Therefore, antibodies attacking cell surface proteins actively, participate in both, tumour elimination and damage of neural tissue. Examples for cell surface proteins involved in PNSs are anti-N-methyl-D-aspartate (NMDA) receptors, alpha-amino-3-hydroxy-5-methyl-4-isoxazolepropionic acid (AMPA) receptors or gamma-aminobutyric acid (AMPA) receptor. [48,82,83] Tumours commonly present in these patients are ovarian, lung and breast cancer, small cell lung cancer and also Hodgkin´s lymphoma.[84]

Antibodies targeting intracellular neuronal protein are also described as onconeural antibodies or "classical paraneoplastic antibodies" and usually imply the presence of an underlying neoplasm. PNSs based on intracellular onconeural antigens, predominantly involve cell-mediated immune responses, whereas antibodies are essential serum markers for PNS diagnosis. As the antibodies have no access to the intracellular antigens, the symptoms are caused by infiltration of CD8+ T cells into the CNS with augmented presence of CTLs in inflamed areas where they actively target and destroy the neurons.[85] Prominent onconeural antibodies are Yo (Purkinje cell cytoplasmic antibody type 1 or PCA-1), Hu, (type 1 anti-neuronal nuclear antibody or ANNA-1) and Ri (type 2 anti-neuronal nuclear antibody or ANNA-2). [82] One of the most investigated paraneoplastic neurological syndromes involving intracellular onconeural antigens is the disorder paraneoplastic cerebellar degeneration (PCD).

3.8. Paraneoplastic Cerebellar Degeneration

PCD is considered as one of the most frequent paraneoplastic syndromes in association with cancer. Characteristic features of PCD are loss of specific neurons located in the cerebellum, called Purkinje neurons, which can eventually result in severe cerebellar ataxia. [86,87] PCD can occur in the presence of any type of cancer, but typically correlates with the presence of small-cell lung cancer (SCLC), gynecologic and breast cancer, and

lymphoma, especially Hodgkin disease. In many PCD cases cancer is diagnosed upon onset of neuropathological symptoms. [88,89]

3.8.1. Pathology

In PCD, tumour cells and Purkinje neurons express the intracellular antigen, referred to as cerebellar degeneration-related antigen (CDR2/CDR2L). High titers of specific antibodies, called Yo-antibodies, against this onconeural antigen are produced and detectable in serum and CSF.[1,90] As described above, effective immune responses against intracellular antibodies in PNSs are predominantly mediated by cytotoxic CD8+ T cells. At early stages of PCD, mild perivascular lymphocytic cuffing, parenchymal microglial activation and CD8+ T cells infiltrating Purkinje cell are observed.[91] A recent study indicates IFN-γ to have striking impact on Purkinje cell death. Besides CD8+ T cells, IFN-γ can be also secreted by macrophages, NK cells, and CD4 Th1 T cells. It changes the metabolism of neurons and attracts phagocytes which in turn produce chemokines and show an upregulation of MHC class I expression in neurons. MHC class I upregulation makes neurons in turn more vulnerable for the attack of cytotoxic CD8+ T cells. In a mouse model the successful treatment with anti-IFN-γ antibody was demonstrated and led to almost complete protection from PCD. This finding again emphasizes CTLs to be the protagonists in the pathomechanism of PCD. The IFN-γ neutralizing antibody suppressed neuronal cell death and hampered T cell infiltrations of the cerebellum.[1] In the late stages of PCD, dramatic or even complete loss of Purkinje cells occurs, thus explaining the low chance of neurological regeneration due to irreversible damage.[92,93]

3.8.2. Clinical Picture

At the beginning of PCD often an impaired balance during walking is noticeable. Some patients also experience dizziness, disrupted motion, ataxic dysarthria (disabilities in speech modulation[94]) or diplopia (double vision[95]). Patients usually experience a deterioration of symptoms over weeks followed by stabilization. At this point of time, patients are usually severely disabled. The majority of patients lose the ability to walk and sit autonomously. Tremor of trunk and head is also observed in PCD patients. Due to dysarthria, patients often lose the ability to communicate effectively, thus triggering isolation and depression. In general, the severity of clinical symptoms varies depending on the type of malignancy and extent of autoimmune reaction. PCD can be mortal within

months, stabilize or even regress. On a neuronal level, the first affected parts in PCD are the vermis and midline cerebellum, but also the cerebellar hemispheres.[86,96–98]

3.8.3. Diagnosis and Treatment of PCD

Tumours that are diagnosed during the course of PCD are histologically malignant and metastases are restricted to a limited area around the tumour. The diagnosis of malignancy is supported by the detection of specific neurological autoantibodies related to distinct cancer types. PCD diagnosis and treatment involve analysis of the patient´s anamnesis, palpation of lymph nodes, breasts and testes as well as rectal and pelvic examination. Antibody screening, MRI scanning and CSF analysis can further help to confirm PCD. If test results are negative, diagnosis of PCD can be based on detection of an underlying tumour or determination of circulating paraneoplastic neuronal autoantibodies (PNAs). However, it has to be considered that diagnosis of PND is still possible, even if all tests are negative. In this case investigations should be repeated every few months. In terms of treatment, currently no effective therapy for PNDs including PCD is approved. For instance, PCD is treated with anti-tumour therapy as regression of malignancy has been observed to result in decrease or at least in stabilization of neurological deficits.[99,100]To achieve the best possible outcome, an early diagnose of cancer and fast introduction of therapy are essential.[1,87]

In consideration of the severity and the lack of treatment of PCD, the protective effect of IFN-γ neutralizing antibody revealed IFN-γ to be a potential target molecule for therapeutic approaches against PCD[1]. As the incidence of PCD increased since the introduction of immune checkpoint-inhibitors[2], the synergic effects of anti-IFN-γ antibody and ICIs might decrease or even prevent ICI side effects which often manifest as PNSs. Therefore, further investigation into the immunological events of PCD under influence of anti-IFN-γ and ICIs is required for a better understanding of the interplay between innate and adaptive immunity.

3.1. L7-HA mouse model

The L7-HA model is used to induce experimental PCD in mice. In this model, the influenza virus protein hemagglutinin (HA) is expressed specifically in Purkinje cells and in mammary cancer cells in the mouse. The pathology of PCD is induced by injecting T cells specifically targeting the HA protein in combination with the immune-checkpoint

inhibitor anti-CTLA4-mAb, which enhances the immune response against the tumour. This overactivation of the immune system also enables T cells to cross the BBB and hence induces a T cell-mediated loss of Purkinje cells resulting in PCD. The L7-HA model was generated by genetic recombination of Rosa-STOP-HA mice and L7-Cre mice. Rosa-STOP-HA mice own a LoxP-flanked stop cassette next to the gene encoding for HA. Hence, in the absence of a cre recombinase, this gene is not expressed in Rosa-STOP-HA mice. L7-Cre mice have a Cre sequence located in the L7/p2p gene which is typically expressed in Purkinje cells in the cerebellum. When these two transgenic mice are crossed, the generated L7-HA mice specifically express the recombinase in the Purkinje cells. The recombinase cuts out the stop cassette and, therefore, HA is expressed in the Purkinje cells of the L7-HA model. [101]

4. Aims of the Thesis

- Analysis of the degree of T cell-mediated neuroinflammation in the cerebellum by immunohistochemistry
- Evaluation of the correlation between pSTAT1 and MHC class I-expression and neurodegeneration by confocal laser fluorescence microscopy
- Identifying inflammatory pathways involved in the pathogenesis of PCD by whole genome transcriptomics with focus on the effect of IFN-γ.

5. Materials & Methods

5.1. Study Samples

Formalin-fixed, paraffin-embedded (FFPE) brain tissue of mice was used. Total number of study samples was 31. Mouse brain and spines were obtained from Prof. Roland Liblau from the Center of Pathophysiology, INSERM, Toulouse. Mice of different genotypes received different treatments (Table1).

Table 1 Overview Study Samples

Sample Number	Genotype	Treatment
511	L7-HA	Anti-IFN-γ, Anti-CTLA4
512	L7-HA	Anti-IFN-γ, Anti-CTLA4
513	L7-HA	Anti-IFN-γ, Anti-CTLA4
514	L7-HA	Anti-IFN-γ, Anti-CTLA4
502	L7-HA	Anti-IFN-γ, Anti-CTLA4
493	L7-HA	Anti-IFN-γ, Anti-CTLA4
95	L7-HA	Control IgG, Anti-CTLA4
113	L7-HA	Control IgG, Anti-CTLA4
121	L7-HA	Control IgG, Anti-CTLA4
122	L7-HA	Control IgG, Anti-CTLA4
130	L7-HA	Control IgG, Anti-CTLA4
137	L7-HA	Control IgG, Anti-CTLA4
138	L7-HA	Control IgG, Anti-CTLA4
139	L7-HA	Control IgG, Anti-CTLA4
240C	L7-HA	-
242	L7-HA	-
239	WT	-
243C	WT	-
292	L7-HA/IFN-γ KO	Anti-CTLA4
310	L7-HA/IFN-γ KO	Anti-CTLA4

311	L7-HA/IFN-γ KO	Anti-CTLA4
313	L7-HA/IFN-γ KO	Anti-CTLA4
272	L7-HA/IFN-γ KO	Anti-CTLA4
Y512/15	WT	-
Y513/15	WT	-
Y514/15	WT	-
Y515/15	L7-HA	CD8+ T cells
Y516/15	L7-HA	CD8+ T cells
Y517/15	L7-HA	CD8+ T cells
Y518/15	L7-HA	CD8+ T cells
Y519/15	L7-HA	CD8+ T cells

Treatments

L7-HA mice received $CD25^{-}CD62L^{+}$ $CD4^{+}$ and $CD62^{+}CD8^{+}$ T cells and 4T1-HA mammary cancer cells on day 0. On the same day, PCD was induced by administration of anti-CTLA-4 mAb which was then injected every other day. Treatments were started on day 10 and were performed intraperitoneally (i.p.) 100µg of anti-IFN-γ mAb (XMG 1.2) was administered every two days. Tumours, weight and neurological symptoms were monitored for a duration of 20 days following sacrifice. [1]

Treatment Groups

Mice were subdivided into different treatment groups. L7-HA anti-IFN-γ group received the anti-IFN-γ mAb after induction of PCD as described above. L7-HA control group received IgG instead of anti-IFN-γ mAb upon induction of PCD. Furthermore, some L7-HA animals neither received anti-CTLA4 mAb, nor did they get any treatment. L7-HA CD8 group received HA-specific CD8+ T cells and IFN-γ-KO mice received IFN-γ deficient T cells.

5.2. Immunohistochemistry of Light Microscopy Staining

5.2.1. Materials

- *3-5µm thick FFPE sections mounted on normal glass slides*
- *Xylene (Avator Materials; Ref. 3410)*
- *Ethanol (EtOH) 96%, 70% and 50% (Brenntag CEE GmbH, Ref. #442269)*
- *TBS-buffer:* TBS-stock solution pH 7.5 (1L): 60,57g of 25mM Tris buffer, 180g of 150mM NaCl and 400ml of 1M HCl were dissolved in deionized water (a.d). The pH was adjusted to 7,5 by adding 1M HCl. TBS working solution: the stock solution was diluted 1:20. 50ml of stock buffer were diluted in 950ml of a.d.
- *PBS-buffer:*
  PBS-stock solution pH 7.4 (2,5L): 13,8g of 0,04M NaH2PO4, 71,2g of 0,16M Na2HPO4 and 90g of NaCl were dissolved in a.d. The pH was adjusted to 7,4.
  PBS working solution: the stock solution was diluted 1:4. 250ml of stock solution were diluted in 750ml of a.d.
- *H2O2/Methanol*: 150mL of Methanol and 1ml H2O2 (30%) were mixed
- *10% FCS/DAKO-Buffer:* the commercial DAKO-buffer solution from Dako corporation 10x (#S3006) was diluted 1:10 with deionized water. For dilution of primary, secondary antibodies and Avidin Peroxidase a solution with 10% FCS in DAKO-buffer was made.
- *EDTA-buffer*
  EDTA 20x stock solution: 1,21g of 10mM Tris-buffer and 0,37g of 1mM EDTA were dissolved in 50ml of a.d. The pH was adjusted to 8,5 or 9,0 depending on fixation of material.
  EDTA working solution: 2,5ml of stock solution was diluted in 50ml of a.d.
- *Peroxidase conjugated Streptavidin 1:500 (Jackson Immunoresearch; #016-030-08)*
- *Catalyzed signal amplification system (CSA):*
- *Biotinylated tyramine stock (CSA-stock*): 6ml of borate buffer (pH=8) (Merck®) was mixed with 15ml of sulpho-NHS-LCS-Biotin (Pierce, Illinois, USA) and 4,5mg of tyramine (Sigma-Aldrich®). The mixture was left overnight at room temperature for stirring and after it was filtered and stored in small aliquots at -20°C.
- CSA working solution: 10µl, 20µl or 50µl of CSA aliquot (1:1500) and 15µl, 30µl or 75µl of H2O2 (1:1000) were mixed with 10ml, 30ml or 75ml of PBS respectively. Both CSA and PBS volumes were chosen according to the amount of slides.

- *Alkaline Posphatase Strepatvidin (AP):* 1:500; Jackson ImmunoResearch
- *Primary antibodies (Table 2)*
- *DAB (3,3'-Diaminobenzidine):* 1ml of DAB (K3467 DAKO®) stock solution was
- mixed in 50ml of PBS. The mixture was filtered with a paper filter into a jar and
- 16,5µl of H2O2 (Merck Millipore) was added.
- Mayers Hemalaun (Merck #1.09249): Mayer´s Hematoxylin (Merck®)
- HCl-ethanol: 100ml of 70% ethanol was mixed with 0,5ml of concentrated HCl (37%).
- Scott's solution: 2g of KHCO3 and 20g of MgSO4 x 7H2O were dissolved in 1.000ml of H2O.
- Coverslips (Carl Roth; H8762)
- Eukitt (Kindler; R1339)

- Primary antibodies:

Table 2 Primary Antibodies for Single Stainings

Antibody	Staining	Antibody Type	Target	Pretreatment	Dilution
pSTAT1	Single	Rabbit monoclonal Ab	Phosphorylated STAT1	EDTA 8.5 60min Steamer	1:2000
CD3	Single	Rabbit monoclonal Ab	T cells	Citrate 60 min Steamer	1:2000

- *Secondary antibodies (Table 3)*

Table 3 Secondary Antibodies for Single Stainings

Antibody	Antibody Type	Dilution
Biotin-Donkey-α-Rabbit	IgG (H+L)	1:1000

Biotin-Donkey-α-Rabbit	IgG (H+L)	1:2000

5.2.2. Method

CD3 and pSTAT1 were stained in all study samples. Brain tissue was cut into 3-5µm thick sections and placed on glass slides. Samples were deparaffinized twice for 15 minutes each in Xylene. Then the slides were washed in 96% ethanol. Endogenous peroxidase was blocked by incubating the slides in a mixture of 0.2% H2O2 in Methanol for 30 minutes. 96% ethanol washing step was repeated followed by immersion into 70%, 50% and aqua destillata (a.d.), hence, achieving rehydration of the tissue. To make the antigen structures accessible for the antibodies, slides were placed into cuvettes filled with EDTA or Citrate and steamed for 1 hour in a household food steamer device (MultiGourmet FS20; Brain, Kronberg/Taunus, Germany). After cooling down, slides were washed 3-5 times with tris-buffered saline (TBS). Next, unspecific binding was blocked by incubation of the samples in 10% FCS (Fetal Calf Serum)/DAKO buffer for 15 minutes. This step was performed in a humid chamber at room temperature to prevent the tissues from drying out. The primary antibodies were diluted in 10% FCS/DAKO buffer, pipetted on the samples and incubated overnight in the fridge at 4°C. The next day, slides were washed 3 to 5 times with TBS to remove the primary antibody. Secondary antibody was diluted in 10% FCS/DAKO, pipetted on the samples and incubated for 1 hour at room temperature. After incubation, slides were again washed 3 to 5 times with TBS. Streptavidin-peroxidase (Jackson) was applied in a concentration of 1:500 diluted in 10% FCS/DAKO for 1 hour. Afterwards, slides were again washed 3 to 5 times with TBS. Stainings were then developed with 3,3´-Diaminobenzidin (DAB) whereas the reaction was stopped with deionized water. Counterstaining was performed by incubating the samples in Mayer´s hemalaun for about 20 to 30 seconds. Samples were then rinsed in tap water and differentiated in HCL-ethanol mixture. Samples were again washed with tap water and then incubated in Scott´s solution for about 2-4 minutes. Washing step in tap water was repeated. The nuclei of the cells were now visible in blue. Dehydration of the tissue was achieved by immersing the slides into ethanol with ascending concentrations including

50%, 70 % and 90% ethanol and n-butyl acetate. Subsequently, coverslips were mounted on the tissue with Eukitt. Samples had to dry about 24 hours and were then studied under the microscope.

5.3. Cell Countings

CD3 and pSTAT1 positive cells in the cerebellum were counted manually by using the 20x objective and an ocular grid. Numbers of Cells/mm^2 was determined for each sample of each group. On average, 30 squares were counted per sample.

5.4. Statistics

For statistical analysis, GraphPad Prism 6 was used to analyse the cell countings. Kruskal-Wallis test in combination with Dunn´s multiple comparison test was performed to compare WT controls to each one of the different treatment groups. Mann-Whitney U test was used to check correlations or differences between Anti-IFN-γ and control IgG treated mice, as well as to compare control IgG treated mice with L7-HA CD8 mice. All p values below 0.05 were considered as statistically significant.

5.5. Confocal Fluorescence Microscopy

Triple stainings of Calbindin, pSTAT1 and β2-MG were performed on two to three samples per treatment group including the samples 121, 122, 311, 512, 511, 239, 243, 313, 310, Y516/15 and Y519/15.

5.5.1. Materials

- 3-5µm thick FFPE sections mounted on normal glass slides.
- Xylene (Avator Materials; Ref. 3410)
- Ethanol (EtOH) 96%, 70% and 50% (Brenntag CEE GmbH, #442269)
- TBS-buffer
- PBS-buffer
- 10% FCS/DAKO-Buffer
- CSA working solution
- Streptavidin conjugated Cy2: 1:100; Jackson ImmunoResearch; #016-220-084
- Gallate/Geltol: 10 ml Geltol + 0.2ml Gallate (0.1M)
- Coverslips (Carl Roth; H8762)
- Confocal LEICA SP5 DMI 6000 CS laser scan microscope (Mannheim, Germany)

- Primary antibodies:

Table 4 Primary antibodies of Triple Staining

Antibody	Types of Staining	Antibody type	Target	Pretreatment	Dilution
pSTAT1	Triple	Rabbit monoclonal Ab	phosphorylated STAT1	Citrate	1:1000
Calbindin	Triple	Rabbit polyclonal Ab	Cal in Purkinje cells	EDTA 8.5	1:1000
β2-MG	Triple	Mouse monoclonal antibody	MHC class I	EDTA 8.5	1:250

- Secondary antibodies:

Table 5 Secondary Antibodies for Triple Staining

Antibody	Antibody Type	Dilution
Cy3-donkey-α-goat	IgG (H+L)	1:100
Cy5-donkey-α-rabbit	IgG (H+L)	1:200
Biotin-donkey-α-rabbit	IgG (H+L)	1:1000

5.5.2. Method

As documented in the method for light microscopy staining samples were deparaffinized with Xylene. Next, they were pretreated with the steamer in cuvettes filled with Citrate for 60 minutes. Slides were then washed with 3 to 5 times with TBS. Sample were then incubated for 15 min with 10% FCS/DAKO diluent in a humid chamber at room temperature in order to block unspecific background reactions. Next, the primary antibody anti-pSTAT1 was diluted in 10% FCS/DAKO diluent and incubated overnight. The next day the applied antibody was gently removed from the slides and again applied and incubated in a humid chamber at room temperature for 1 hour. Next, the slides were

washed with TBS and the biotinylated secondary antibody diluted in 10% FCS/DAKO buffer was applied. Samples were incubated for one hour at room temperature in a humid chamber. Samples were then incubated with peroxidase-conjugated streptavidin diluted 1:500 in 10% FCS/DAKO buffer. Samples were then incubated in CSA working solution for 20 minutes at room temperature. Next, the slides were again steamed in EDTA-filled cuvettes (pH = 8.5) for 30 minutes. The primary antibodies β2-MG and Calbindin were then applied and incubated overnight in a humid chamber at 4°C in the fridge. The next day, all secondary antibodies and Streptavidin conjugated Cy2 were applied and samples were incubated 1 hour at room temperature. The last step included mounting the samples with cover slips fixed by Geltol/Gellate. Flourescent preparations were examined using the confocal LEICA SP5 DMI 6000 CS laser scan microscope. Three different lasers were used including Argon laser with excitation Line (EL) at 475nm and Emission Peak (EM) at 510nm, DPSS561 laser with EL at 561nm and EP at 570nm and HENe 633 with EL at 633nm and EP at 670 nm.

5.6. RNA isolation

5.6.1. Materials

- 8 µm FFPE sections (RNase-free) mounted on normal glass slides
- Fume hood (SM Labortechnik), RNase-free space
- 55°C and 70°C incubator (Heraeus Instruments – Thermo Electron Corporation)
- High Pure FFPE RNA Micro Kit (Roche, Ref. #04823125001)
- Xylene (Avator Materials)
- EtOH absolute (Merck Millipore, #64-17-5)
- EtOH 96%, 70% (Brenntag CEE GmbH, 442269)
- Lysis buffer per isolation: 60 µl buffer + 10 µl 10% SDS
- RNase ZAP (Life Technologies, AM9780)
- RNase-free H_2O (Gibco, Life Technologies, 10977)
- 10% SDS (Alfa Aesar, 1711183)
- RNase-free 1.5 ml Eppendorf tubes
- RNase-free 0.6 ml Eppendorf tubes (Biozym, 710300)

- Surgical disposable scalpels (Braun Aesculap Division, #5518091)
- Vortex Mixer 7-2020 (neoLab; Ser.-Nr. 000769)
- Centrifuge 5415D (Eppendorf)
- Centrifuge Sigma 1-14 (Linder Labortechnik)

FFPE-Tissue

All methods performed were based on formalin fixed paraffin embedded tissue (FFPE) samples from mouse cerebella showing different extents of PCD pathology due to distinct treatments. FFPE tissue was used as this preservation method enables storage over a long period of time and does not require cost-intensive storage conditions. Furthermore, formalin maintains cellular structures very well as it establishes cross links between nucleic acids and proteins. Although proteins and cellular structures are well preserved, investigations on a molecular level were challenging. FFPE tissue exhibits many modifications on nucleic acids and proteins due to fixation, including denatured proteins and breaks in the sugar-phosphate backbone of the DNA/RNA through hydrolysis of phosphodiester bonds. Hence, RNA of FFPE tissue is often quite fragmented which makes it more difficult to isolate a proper amount of good-quality RNA[102]

5.6.2. Method

Before procedure of RNA isolation was started, working bench, tables, pipettes, and further equipment was cleaned with RNase Zap® and 70% Ethanol. Proteinase K aliquot was thawed and kept on ice. The cerebellum was cut out with a scalpel and deparaffinized in a 0.5 ml Eppendorf tube with 800µl Xylene. Samples were vortexed 3 times for 4 seconds and incubated for 2 minutes at room temperature. The vortex step was repeated, and samples were incubated for 5 minutes at room temperature. Samples were spun down at full speed (13.200 rpm) in the centrifuge for 2 minutes. The Xylene was then removed without disturbing the pellet. Xylene steps were repeated. Next, 800µl of Ethanol absolute was added to each sample. The vortex step (3x4sec) was repeated and samples were spun down at full speed for 2 minutes. Next, 800µl of 70% Ethanol was added to each sample and samples were spun down for 2minutes. Ethanol was removed as much as possible and samples were spun down again for 30 seconds. Ethanol leftovers were removed and Eppendorf tubes were positioned in a pipette tip box with lid open and incubated at 55°C in the incubator till Ethanol had evaporated from the tissue. After

air drying 70µl of lysis buffer per sample was added. 30µl Proteinase K was then added to each sample the suspension was mixed thoroughly by pipetting up and down. Samples were then again positioned in a pipette box and incubated at 55°C for 3 hours in the incubator. After 3h, an additional heating step of 70°C for 20 minutes was performed to increase the RNA yield and resolve possible left-over crosslinks from formalin fixation. After incubation 200µl binding buffer and 200µl 100% Ethanol were added to each sample. Samples were vortexed for 4 seconds and spun down shortly. A filter tube was then combined with a collection tube. The lysate was pipetted into the upper reservoir and samples were then vortexed with 8000xg for 30 seconds. The flow-through was then discarded and samples were again spun down at maximum speed for 1 minute. 30µl of DNase Solution (3µl + 27µl DNase I) per sample was added in order to remove genomic DNA and incubated for 15 minutes at room temperature. Three washing steps followed in order to purify the RNA. First, 300µl of washing buffer I was added to each sample. Samples were vortexed with 8000xg for 15 seconds. The flow-through was discarded. Then 300µl of Wash Buffer II was added to each sample and samples were vortexed again at the same speed as before. Flow-through was discarded and 200µl of Wash Buffer II were added and the centrifugation step was repeated. Flow-through was discarded and filter tubes were placed into fresh collection tubes. Samples were now centrifuged at maximum speed for 2 minutes. Filter tubes were placed in a fresh 1.5ml Eppendorf tube. 20µl Elution buffer per sample were added and tubes were incubated for 1 min at room temperature. Samples were centrifuged at with 8000xg for 1 minute and the eluate was reloaded to increase the RNA yield. Samples were again incubated for 1 minute at room temperature. Now samples were centrifuged with 8000xg for 1 min and then with maximum speed for 2 minutes in order to get rid of disturbing glass fibers at the bottom. The eluate was aliquoted and transferred in a new 0.5 ml Eppendorf tube and samples were stored at -80°C.

5.7. RNA Quality and Quantity Control

RNA quality and quantity were assessed to control the suitability for microarray analysis. Two approaches were taken to control RNA quality. First, RNA concentration and quality was examined by application of Agilent 2100 Bioanalyzer (Agilent Technologies) and

usage of the Agilent RNA 6000 Pico Kit (Agilent 6000). Secondly, qPCR was performed upon conversion of RNA into cDNA using the iScript™ cDNA Synthesis Kit (Bio-Rad).

5.7.1. Agilent 2100 Bioanalyzer

With this method the concentration and percentage of fragments over 200 base pairs (DV200) was measured and all samples containing more than 660pg/µl and a DV200 over 60% were analysed in further quality steps. The concentration was analysed by the 2100 Expert software.

5.7.1.1 Materials

- Agilent RNA 6000 Pico Kit containing: 25 RNA Pico Chips, 3 Electrode Cleaners, Syringe Kit, 1 Syringe, Tubes for Gel-Dye Mix, 30- Safe-Lock Eppendorf Tubes PCR clean (DNase/RNase free) for gel-dye mix

5.7.1.2 Method

Firstly, the RNA ladder was spun down and pipetted into a RNase-free vial. The ladder was denatured for 2 minutes at 70°C then. Afterwards the vial was immediately put on ice. Then 90µl of RNase-free water was added and mixed thoroughly. Subsequently, the ladder mix was aliquoted into 0.5ml RNase-free vials and stored at -70°C. Before use the ladder was thawed on ice. The gel was prepared by pipetting 550µl of the RNA gel matrix into a spin filter. The tube was spun with 1500g ±20% for 10 minutes at room temperature. The filtered gel was then aliquoted into 0.5ml RNase-free microcentrifuge tubes. Gels were stored at 4°C and used within 4 weeks. Before starting the procedure, RNA dye concentrate should equilibrate to room temperature for 30 minutes. Then RNA dye concentrate was vortexed for 10s, spun down and 1µl of dye was added to a 65µl aliquot of filtered gel. Solution was vortexed thoroughly and tube was spun at 13000xg for 10 minutes at room temperature. Samples were then put from the freezer on ice and kept there during the whole procedure. A new RNA chip was put on the priming station. 9µl of gel-dye mix was pipetted in the well-marked G on the chip. A plunger was used to press the gel-dye mix into the wells. The remaining gel-dye mix was discarded. Next, the conditioning solution and marker were loaded. 9µl of the RNA conditioning solution were pipetted into the well-marked with CS. Then 5µl of RNA marker was pipetted in all 11 sample wells and in the well-marked with a ladder. Finally, the diluted ladder and the samples were loaded. 1µl of the heat denatured and aliquoted ladder was pipetted into

the well-marked with a ladder. 1µl of each sample was pipetted into each of the sample wells. In case some wells were not used, 1µl of RNA marker was added in these positions. The chip was put horizontally in the IKA vortexer and was vortexed for 1 minute at 2400rpm. The chip was then analysed by the Agilent 2100 Bioanalyzer instrument within approximately 30 minutes. The program automatically calculated the DV200 number and, on the basis of that, presented a correlating graph (Figure 6).

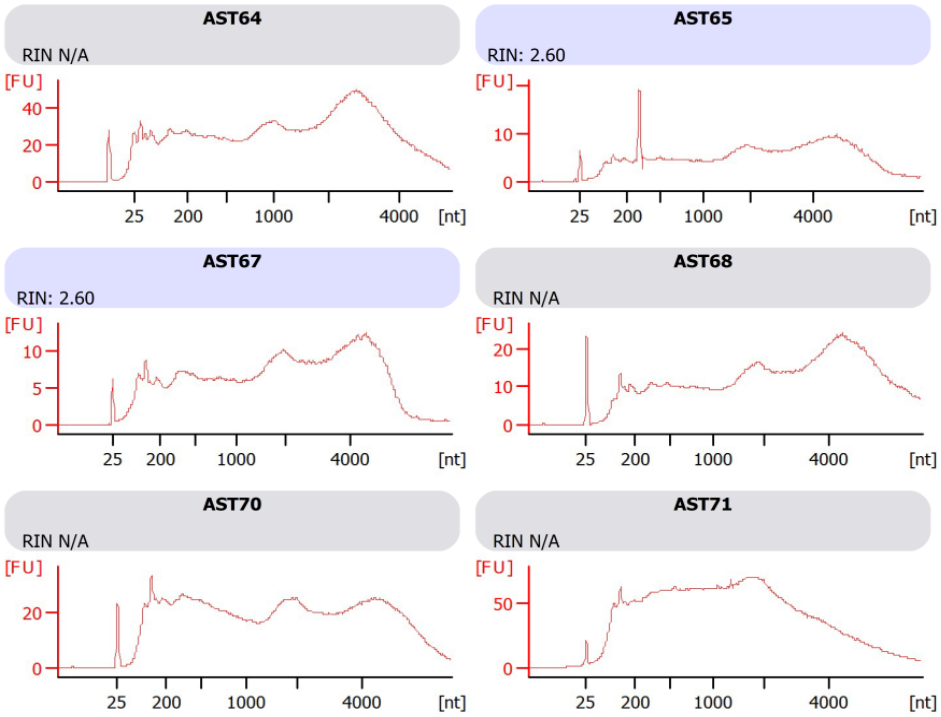

Figure 6 Representative Plots of RNA Sample Concentration
RNA of FFPE-fixed tissue of mouse brains was isolated and controlled qualitatively and quantitatively by Bioanalyzer analysis. All samples showed a concentration over 600pg/µl and were therefore suitable for microarray analysis.

5.7.2. cDNA synthesis

For the performance of qPCR, RNA had to be converted into cDNA. The cDNA is used as a template for the DNA amplification by the DNA-Polymerase.

5.7.2.1. Materials

- Fume hood (Holter LaminAir)
- Vortex Mixer 7-2020 (neoLab, Ser.-Nr. 000769)
- MyFuge™ Mini centrifuge (Benchmark Scientific C1008-B*)

- iScript™ gDNA clear Synthesis Kit (Cat. #170-8891):

  - iScript Rverse Transcription Supermix

  - iScript No-RT Control Supermix

  - iScript DNase, iScript DNase Buffer

  - Nuclease-Free Water
- My Cycler™ Thermal Cycle (BIO-RAD Laboratories)
- PCR soft tubes 0.2ml DNase/RNase Free (Biozym Biotech Trading GmbH, Art.-Nr.710908)
- RNase-free 1.5ml Eppendorf tubes
- RNA samples

5.7.2.2. Method

The procedure of cDNA synthesis again performed under RNase free conditions. First DNase master mix was prepared by combining proper amounts of DNase and iScript DNase Buffer to remove any left-over gDNA (Table 6). Master mix was mixed by pipetting up and down thoroughly. Then deionized water was added to the RNA samples to reach a concentration of 4ng and a final volume of 20µl. To control the RNA samples for contamination with gDNA, a no-RT control supermix was used. DNase-treated RNA was then mixed with Reverse Transcription Supermix (Table 7). Finally, all samples were positioned in the thermal cycler with the heated lid on and incubated according to the guidelines in Table 8.

Table 6 Setup for DNase master mix

Components	Volume per Reaction [µl]	Ten Reactions [µl]
iScript DNase	0.5	5
iScript DNase Buffer	1.5	15
Total Volume	2	20

Table 7 DNase reaction protocol

Step	Temperature, °C	Time, min
Priming	25	5

Reverse transcription	46	20
RT inactivation	95	1
Hold (optional)	4	-

Table 8 Setup for cDNA synthesis reaction

Component	Volume per Reaction [µl]
iScript Reverse Transcription Supermix	4
DNase-treated RNA template	16
Total volume	20

5.7.3. qPCR

As FFPE – tissue is often quite fragmented and modulated due to its fixation, the converted cDNA is often not accessible for the enzymes involved in further analysis steps (REF), e.g. the Polymerase in qPCR. Proper amplification of the cDNA in the context of Real-Time Polymerase Chain Reaction (RT-PCR or qPCR) is a good indicator for the RNAs suitability for microarray analysis.

5.7.3.1. Materials

- My Fuge™ Mini Centrifuge (Benchmark Scientific, C1008-B*)
- StepOnePlus Real-Time PCR System (AB Applied Biosystem)
- Vortex Mixer 7-2020 (neoLab; Ser.-Nr. 000769)
- Fume hood (Holter LaminAir)
- SsoAdvanced™ Universal SYBR® Green Supermix (Catalog #172-5271)

PCR soft tubes 0.2ml DNase/RNase Free (Biozym Biotech Trading GmbH; Art.-Nr. 710908)

- Multiplate® PCR Plates™ 96-wells (BIO-RAD Laboratories)
- Microseal® ´B´seal Seals (BIO-RAD Laboratories, Cat. MLL9601)
- RNase-free 1.5 ml Eppendorf tubes
- RNase-free H2O (Gibco, LifeTechnologies, Ref. #10977)
- Real-Time PCR Primers (Table 9)

Table 9 Mouse Primer for qPCR

Gene	End	Efficiency	Forward Primer	Reverse Primer
GAPDH 3´	3´end	96%	GGTATGACAATGAATACGGCT	GTCCAGGGTTTCTTACTCCT
HPRT1	middle	93%	TGTTGTTGGATATGCCCTTG	TTGCGCTCATCTTAGGCTTT

5.7.3.2. Method

The method of qPCR was used to quantify the expression of the mouse housekeeping genes encoding for Glyderaldehyde-3-phosphate dehydrogenase (GAPDH) and Hypoxanthine-guanine phosphoriosyltransferse (HPRT1). GAPDH3´ bound to the 3´end whereas HPRT1 bound in the middle of the DNA. First a master mix, consisting of SsoAdvancedTM universal SYBR® Green supermix, forward and reverse primer and nuclease-free water, was prepared. Then 9µl of the master mix were pipetted in each well of the Multiplate®PCR Plates™96 – wells. Next, 1µl of each cDNA sample was added in triplicates. The total volume per well amounted to 10µl (Table 10). In the negative controls 1µl of H2O was added instead of cDNA to control potential contaminations of the master mix RT (Reverse Transcriptase) controls were used to check samples for contamination with genomic DNA. Then the plate was sealed with an adhesive foil and vortexed shortly. Afterwards, the plate was shortly spun down at 4°C in the centrifuge for air bubble removal and proper collection of the reaction mix on the bottom of the wells. The plate was inserted into the RT-PCR System and qPCR was started and performed by the RT-PCR system and in consideration of the recommended thermal cycling protocol of the manufacturer (Table 11). Data analysis was performed with the Applied Biosystems StepOneSoftware 2.3 and threshold was set to 0.3 for all amplifications.

Table 10 Reaction setup for RT-PCR

Component	Volume per 10µl Reaction [µl]	Final Concentration
Sso Advanced universal SYBR® Green Supermix	5	1x
Forward primer	0.2	200nM
Reverse primer	0.2	200nM
Template (cDNA)	1	200pg
Nuclease-free H2O	3.6	-
Total reaction mix volume	10	-

Table 11 Thermal cycling protocol for RT-PCR

Real-Time PCR System	Setting/Mode	Polymerase Activation and DNA Denaturation	Amplification			Melt-Curve Analysis
			Denaturation at 95°C/98°C	Annealing/Extension + Plate Read at 60°C	Cycles	
ABI7500, StepOne, StepOnePlus, 7900HT and ViiA7	Standard	30 sec at 95°C for cDNA	15 sec at 95°C	30 sec	50	65°C-95°C 0.5°C increment 2-5sec/step (or use instrument

						default setting)

5.8. Affymetrix GeneChipTM whole-genome microarrays

Microarrays were performed by Markus Jeitler, Bsc from the core facility for genomics of the Medical University of Vienna. For the analysis, samples were hybridized with a RNA GeneChip^{TM}Mouse Gene 2.0 ST Array. Gene TitanTM MC Instrument (Affymetrix, Thermo Fisher Scientific) was used to scan the array.

5.8.1. Microarray Quality Control

Transcriptome analysis software TAC 4.0 was used to check data distribution of raw data (CEL files). Upon RMA-normalization (CHP files), brightness/darkness of array was checked to detect potential outliers. Furthermore, the array was checked for probeset-mean (pb-mean) and the background-mean (bgrd-mean) to determine the signal-to-noise ratio, which helps to distinguish between positive and negative signals. Furthermore, mean absolute deviation (mad) residual mean was checked to assess the difference between expected and mean value. Relative log expression (rle) mean showed the general deviation of a sample in comparison to all arrays. Next, positive versus negative AUC described the level of discrimination between positive and negative signals, whereas AUC = 1 accounts for a perfect discrimination and 0.5 accounts for totally random signals. Considering the AUC range of FFPE tissue, results above 0.65 are acceptable. Genes with a ± fold change of 2 and a FDR of 0.05 were further investigated and, hence, exported to gene set enrichment analysis program gProfiler[103].

5.8.2. Microarray Analysis

Microarray analysis was performed according to Raimand et al 2019: Differentially expressed genes were ranked according to –log10(p-Value)*fold-change. The higher the p-Value and fold change, the higher the rank. Then the ranked gene list was exported into gprofiler and gene sets from GO:biological function and reactome were used to identify enriched pathways. GEM and GMT files were downloaded and an enrichment map was generated with the program cytoscape v.3.8.0. The map was adjusted for better visualization with a node-cut off of 0.7 and an edge cut off of 0.5718. Annotations of each cluster were done with the “auto-annotate” app from cytoscape.[103]

6. Results

6.1. High Variability of T cell activity in the different groups detected by qualtitative and quantitative Analysis of CD3 and pSTAT1 Light Microscopy Stainings

As T cells are highly active upon ICI treatment, they can more easily cross the BBB and, in case of epitope recognition, lead to severe neuronal loss.[1,101] To determine the degree of brain Under physiological conditions, hardly any T cells are found in the brain[104]. However, in case of PCD, increased T cell numbers are found in the brain parenchyma close to Purkinje neurons[1]. In the L7-HA model, T cells were specific for L7-HA expressing Purkinje cells, hence, they induced T cell-mediated neuronal loss specifically in these cells.[101] Markers for CD3 and pSTAT1 were used to analyse and compare T cell infiltrations in the cerebella of the different treatment groups. In WT mice hardly any T cells were detected in the cerebellum. In the IFN-γ-KO mice and L7-HA CD8 model T cells were detected in close proximity to Purkinje neurons and spread throughout the parenchyma. A similar pattern of T cell infiltration was observed for conIgG treated animals. Interestingly, anti-IFN-γ treated animals showed far less neuroinflammation than the other groups (Figure 7).

Further, CD3 positive cells of all groups were quantified. Significant differences were shown between wildtypes (WT) compared to conIgG, IFN-γ-KO and L7-HA CD8. Anti-IFN-γ did not significantly differ from WT (Figure 8A). CD3 cell numbers of samples used for microarray analysis showed similar significances and WTs showed no CD3 positive cells in the cerebellum whereas conIgG, IFN-γ-KO and L7-HA CD8 animals showed increased T cell numbers. There was no significant difference between anti-IFN-γ and WT (Figure 8B).

Moreover, we wanted to identify the activity of the T cells by analysing the degree of IFN-γ signalling by staining for pSTAT1. The marker was chosen as IFN-γ is the predominant cytokine secreted by CD8+ T cells and uses the JAK-STAT pathway to promote inflammation[105]. IFN-γ alters the cell´s gene expression and leads to an upregulation of MHC class I molecules on the cell´s surface. Consequently, neurons become more vulnerable to the cytotoxic action of CD8+ T cells.[1] Hence, the extent and area of inflammation could be assessed by using the marker pSTAT1. In WT mice no pSTAT1

positive cells could be detected. In IFN-γ-KO, conIgG and L7-HA CD8 mice pSTAT1 was detected primarily in Purkinje cells and the molecular layer with increased density close to the Purkinje cell layer. In the molecular layer, pSTAT1 positive cells predominantely exhibited an astrocytic morphology, but also dendritic shapes as seen in microglial cells. Anti-IFN-γ animals showed very small amounts of pSTAT1-positive cells compared to IFN-γ-KO, con IgG and L7-HA CD8 mice.

Samples with pSTAT1 positive cells revealed significant differences between WT and conIgG as well as WT and IFN-γ KO animals. No significant difference was neither observed between WT and anti-IFN-γ, nor between WT and L7-HA CD8 (Figure 8C). Neither did cell number differ significantly between WT and anti-IFN-γ, nor between WT and L7-HA CD8 (Figure 8D). The comparison of pSTAT1 positive cells between anti-IFN-γ and conIgG revealed a significant higher cell number in conIgG animals than in anti-IFN-γ animals. Similar to that, conIgG animals also showed a higher number of CD3 positive cells than anti-IFN-γ group did (Figure 8G). Positive control conIgG and untreated L7-HA CD8 animals showed no significant difference in their CD3 positive cell number and, hence, the analyses of differentially expressed pathways were done with the conIgG group, which passed all quality checks (Figure 8F). General interaction of CD3 with pSTAT1 was compared within the different groups and revealed significant difference between WT and IFN-γ-KO (Figure 8H). Linear regression of CD3-pSTAT1 interaction was analysed and showed significance in conIgG (Figure 8I). To sum up, both, CD3 and pSTAT1 cell numbers were significantly higher in the groups of conIgG, IFN-γ-KO and L7-HA CD8 compared to WT animals. Interestingly, anti-INF-γ treated animals showed a significant lower number of infiltrating T cells as well as T cell activation, with levels comparable to WT animals.

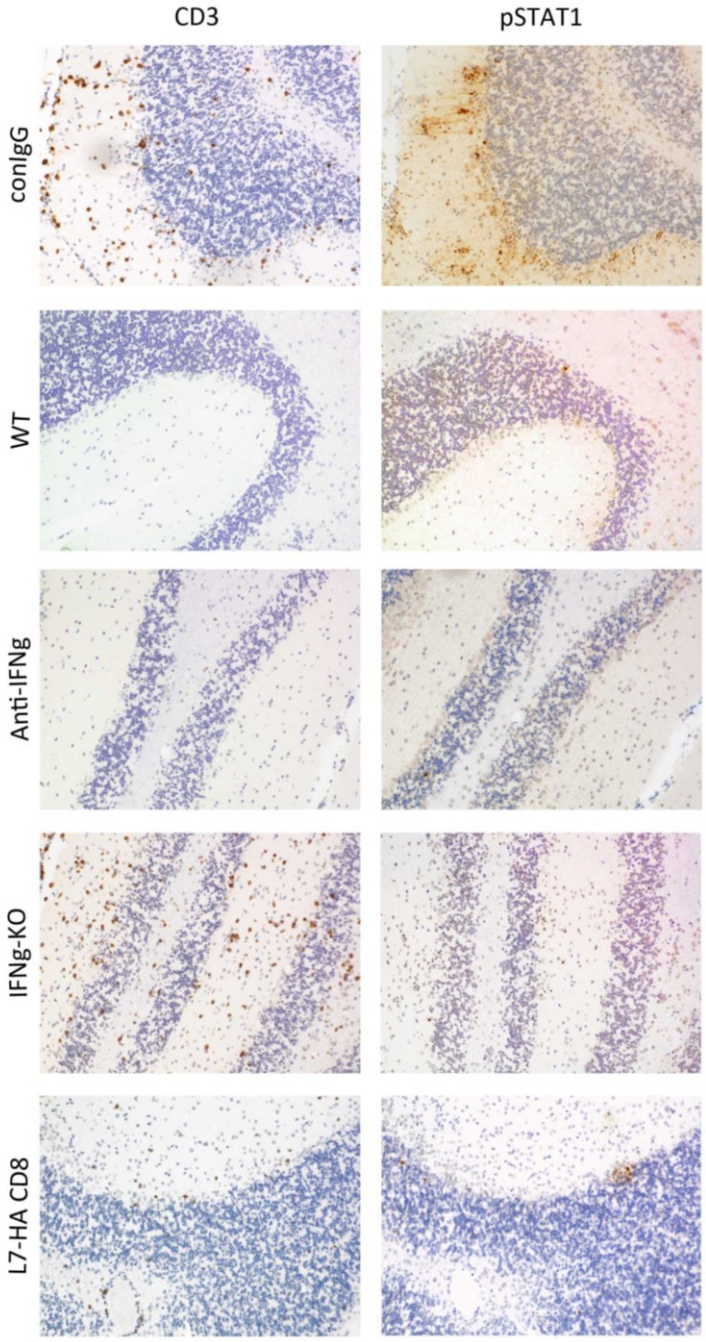

Figure 7 CD3 and pSTAT1 stainings

Samples of all groups were stained with CD3 and pSTAT1 to assume the extent of T cell infiltration and inflammatory activity. Labelled cells are visible in brown.

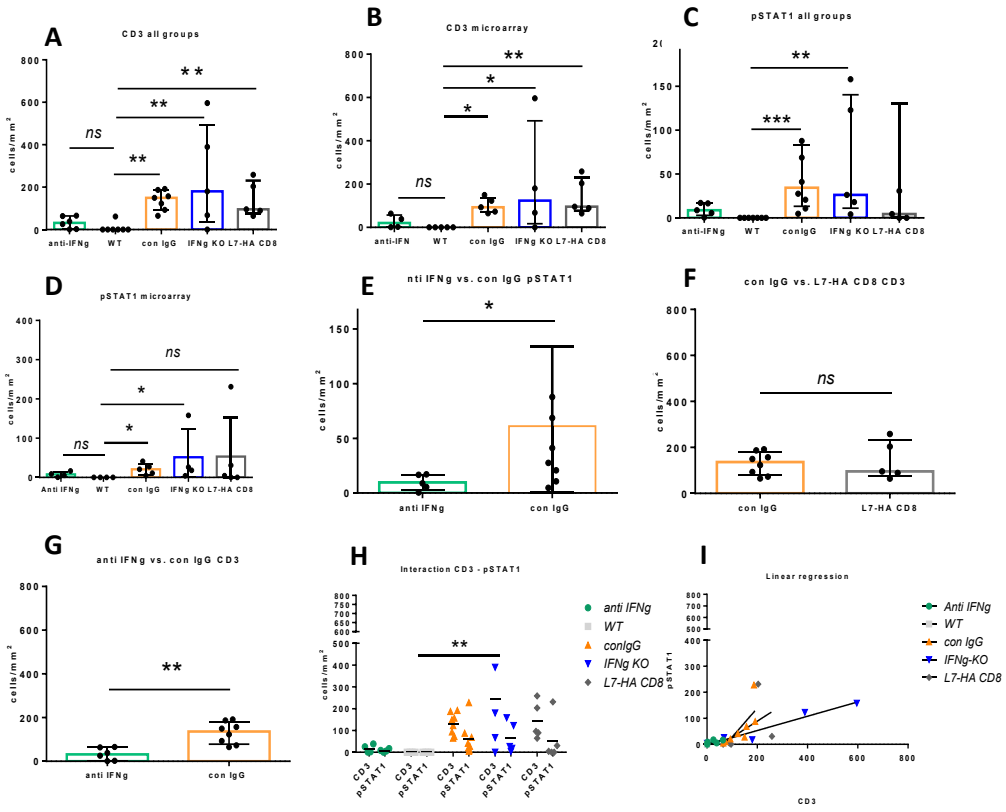

Figure 8 Comparative Analysis of Cell Quantifications

A: Comparison of CD3 cell counts of each treatment group. (Median; Inter-Quartile Range (IQR); Kruskal-Wallis test with multiple comparison; n=30; p=0.0009), **B:** Comparison of CD3 cell counts of each treatment group used for microarray analysis. (Median; IQR; Kruskal-Wallis test with multiple comparison; n=23; p=0.0061),**C:** Comparison of pSTAT1 cell counts of each treatment group (Median; IQR; Kruskal-Wallis test with multiple comparison; n= 31; p=0.0022), **D:** Comparison of pSTAT1 cell counts of each treatment group used for microarray analysis (Median; IQR; Kruskal-Wallis test with multiple comparison; n=22; p=0.0514), **E:** pSTAT1 cell numbers of anti-IFN-γ and conIgG were compared. (Mann-Whitney U test; IQR; n=13; p=0.0451), **F:** CD3 cell numbers of conIgG and L7-HA CD8 were compared. ConIgG served as positive control for treated L7-HA animals. L7-HA CD8 animals received no treatment. (Mann-Whitney U test; IQR; n=13; p=0.9293), **G:** CD3 cell numbers of anti-IFN-γ and conIgG were compared. (Mann-Whitney U test; IQR; n=14; p=0.0013), **H:** Overall interaction of CD3 with pSTAT1 in different treatment groups. (2way ANOVA with Sidak´s multiple comparison; n=36, Interaction p = 0.0424, Staining p = 0.0006, Treatment p = 0.0463, Subjects matching p = 0.0037), **I:** Correlative relationship between CD3 and pSTAT1. (Spearman Correlation of Linear Regression; n=54 ; r=0.5000; conIgG p = 0.0011

A-I: Green = anti-IFN-γ ; light grey = WT; orange = conIgG; blue = IFN-γ-KO; dark grey = L7-HA CD8

****p < 0.0001; ***p < 0.001; **p < 0.01; *p < 0.05

6.2. Analysis of MHC class I and pSTAT1 expression in Correlation with Neurodegeneration by Confocal Laser Flourescence Microscopy

The aim of this procedure was identifying the interaction of IFN-γ signalling, MHC-I upregulation and the degree of neurodegeneration. Hence, triple stainings were performed on three samples per treatment group. The interplay between pSTAT1 positive cells labelled green, MHC class I molecules labelled with β2-microglobulin (β2-MG) in red and the presence or absence of healthy neurons stained with calbindin in blue was analysed. Pictures of the stainings were taken and representatives for each treatment group were chosen (Figure 9).

Wildtype animals showed normal physiological healthy amounts of calbindin positive neurons which formed a uniform layer of Purkinje cells throughout the cerebellum (Figure 9C, G). There was no β2-MG reactivity and no pSTAT1 positive cells. Anti-IFN-γ treated animals showed an equal distribution of calbindin positive neurons and moderate β2-MG reactivity. However, hardly any pSTAT1 positive cells were detected (Figure 9B, F). ConIgG, IFN-γ-KO and L7-HA CD8 animals (Figure 9J, N, R) showed severe neuronal loss of calbindin positive Purkinje cells, with parts of the cerebellum completely rid of these cells. Moreover, β2-MG was highly upregulated in the granular and molecular cell layer of the cerebellum. PSTAT1 reactivity was strongly present in the Purkinje cell layer as well as the molecular cell layer. WTs did not exhibit pSTAT1 positive cells at all (Figure 9A) and anti-IFN-γ animals showed complete absence or very small numbers of pSTAT1 positive cells (Figure 9E). In contrast, conIgG and L7-HA CD8 animals in general showed quite high numbers of pSTAT1 positive cells accompanied by increased numbers of MHC class I molecules and a smaller amount of healthy calbindin positive neurons compared to WT and anti-IFN-γ animals (Figure 9I-P). IFN-γ-KO animals showed a great variability in their pSTAT1 positive and β2-MG positive cells ranging from very high to very low amounts (Figure 9 Q-T). The striking differences between anti-IFN-γ and conIgG is again demonstrated in Figure 10.

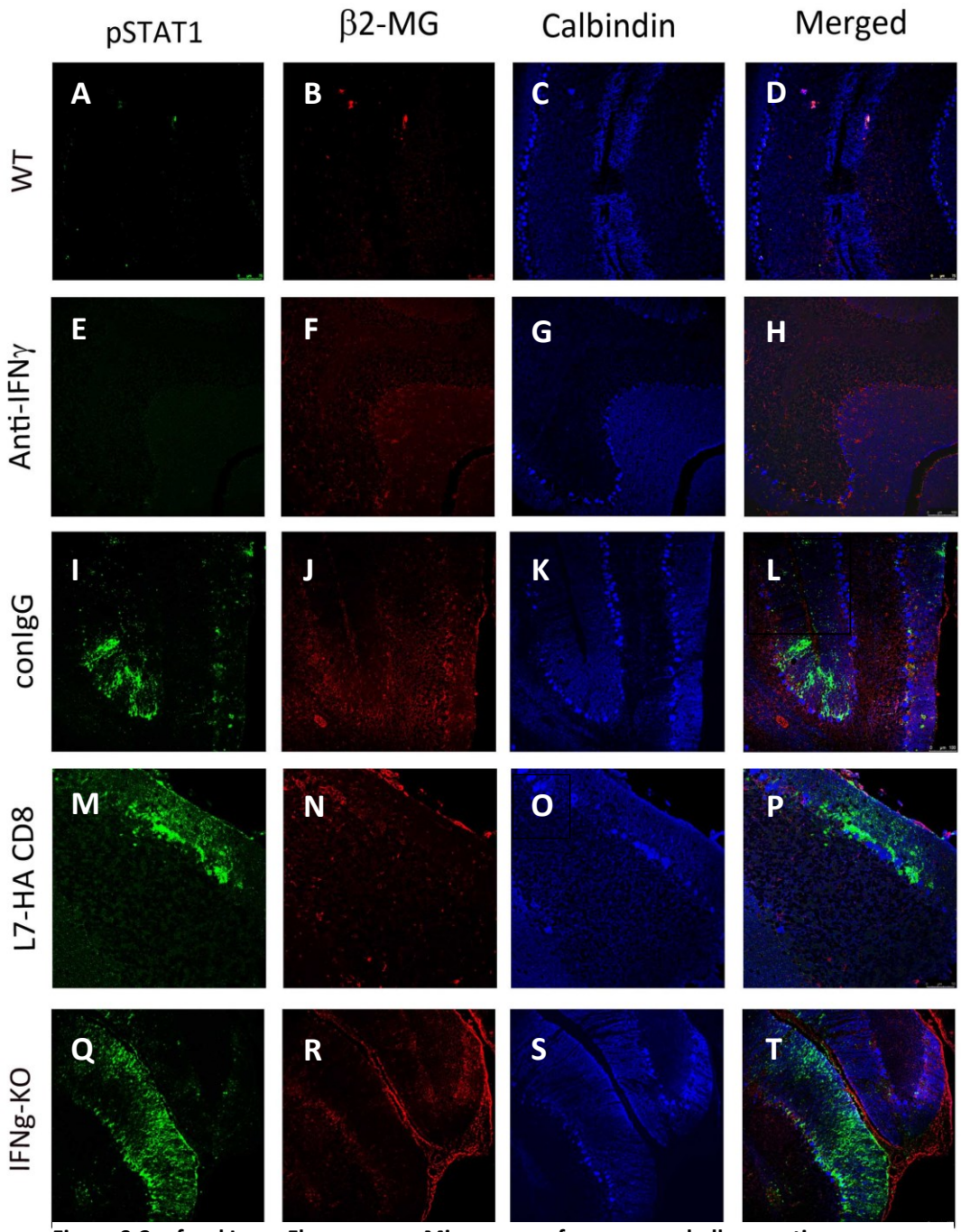

Figure 9 Confocal Laser Flourescence Microscopy of mouse cerebellum sections

A-Q: Cells stained with pSTAT1 are visible in green. **B-R:** Cells labelled with β2-MG are shown in red.

C-S: Calbindin positive cells are presented in blue. **D-T:** Overlay of the single colour channels.

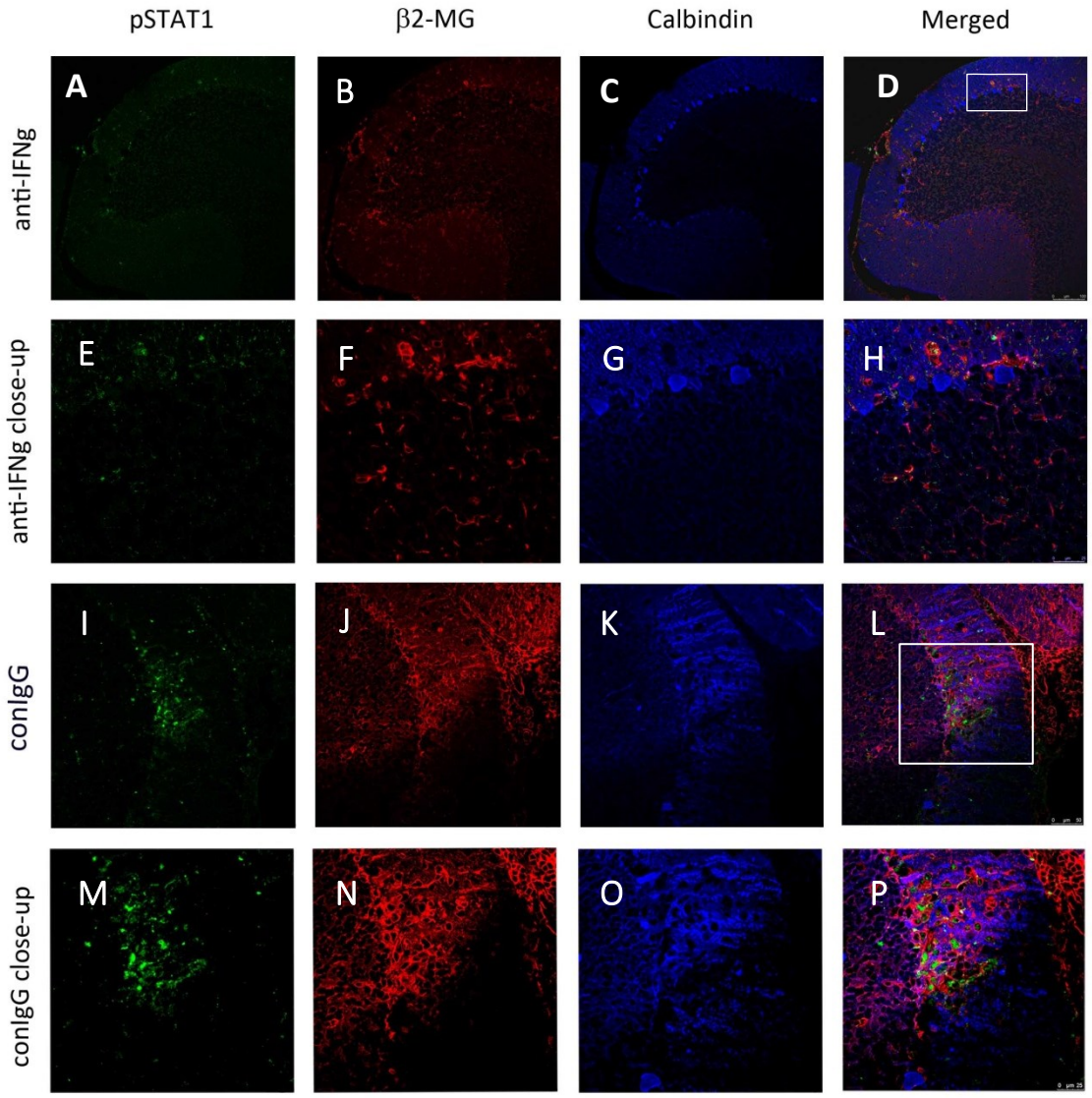

Figure 10 Confocal Laser Flourescence Microscopy of anti-IFN-γ vs. con IgG

A-M: Cells labelled with pSTAT1 are shown in green. **B-N:** Cells labelled with β2-MG are shown in red. **C-O:** Cells labelled with Calbindin are shown in blue. **D-P:** Overlay of the single colour channels.

6.3. Microarray Quality Control

The control of the metric quality was an essential step to determine the samples suitable for further analysis steps. Control parameters including AUC, RLE mean, mad residual mean, probeset mean and background mean were checked. Probeset signals (outliers excluded) were visualized before normalization and after normalization (Figure 11). Probeset mean and background mean were analysed via Affymetrix Expression Console™ before normalization of sample data (Figure 12). The AUC for all samples was detected in a range between 0.60 and 0.72. Three samples of the WT group and all L7-HA group showed an AUC of only around 0.6, which is not considered a good enough discrimination between positive and negative signals. All other samples ranged between 0.65 and 0.72, which was interpreted as good signal discrimination (Figure 13A). The RLE mean and the MAD residual mean showed unusual high values and unexpected deviations in the same three WT and all L7-HA samples. All other samples showed low RLE mean and MAD residual mean, indicating good data reliability (Figure 14A). Therefore, Microarray quality control detected three samples in the group "WT" and all samples of "L7-HA CD8" as outliers. Hence, they were excluded from gene expression analysis and quality control was repeated (Figure 11-14 panel B in each Fig). Normalization of the remaining samples was repeated after exclusion of the outliers, which improved the signal-to-noise ratio (11B).

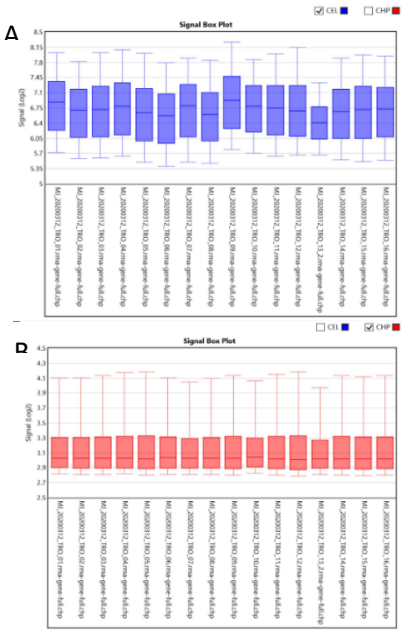

Figure 11 Signal Box Plots before (CEL) and after normalization (CHP)

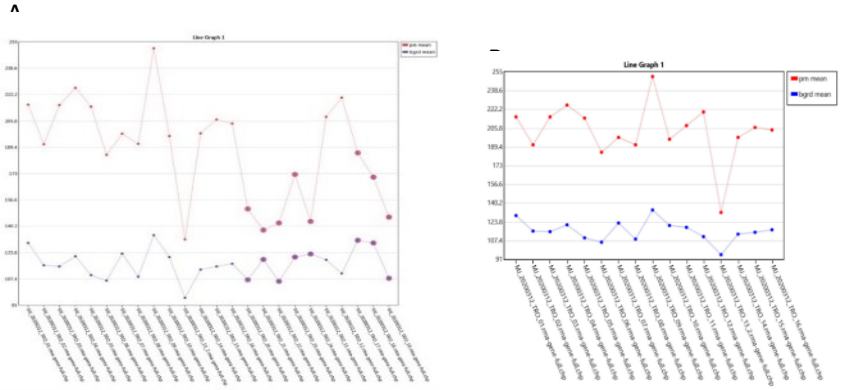

Figure 12 Probeset mean and Background mean of probes with and w/o outliers

A, B: The probeset mean (red) consists of all perfect match probes on the array and helps to detect striking bright or dim arrays. The background mean (blue) shows the mean signals resulting from non-genomic array reactions and is also used to analyse bright and dim arrays. Both means are independent from other arrays.
A: Data including outliers. Outliers are labelled in pink/violet. B: Data exdcluding outliers.

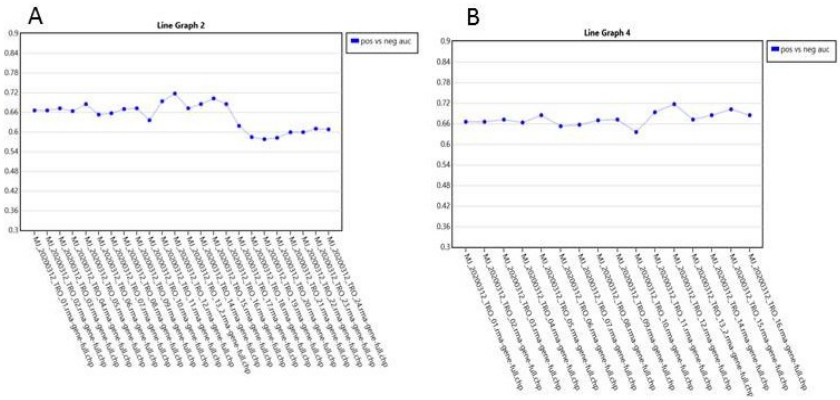

Figure 13 Negative vs. positive AUC w/o outliers

The AUC compares data of positive and negative signals and allows to evaluate their distinction. An AUC of 0.5 displays no separation between positive and negative signals. An AUC of 1 shows perfect discrimination of the signals.
Left figure (A) shows AUC with outliers. Right figure (B) shows AUC without outliers.

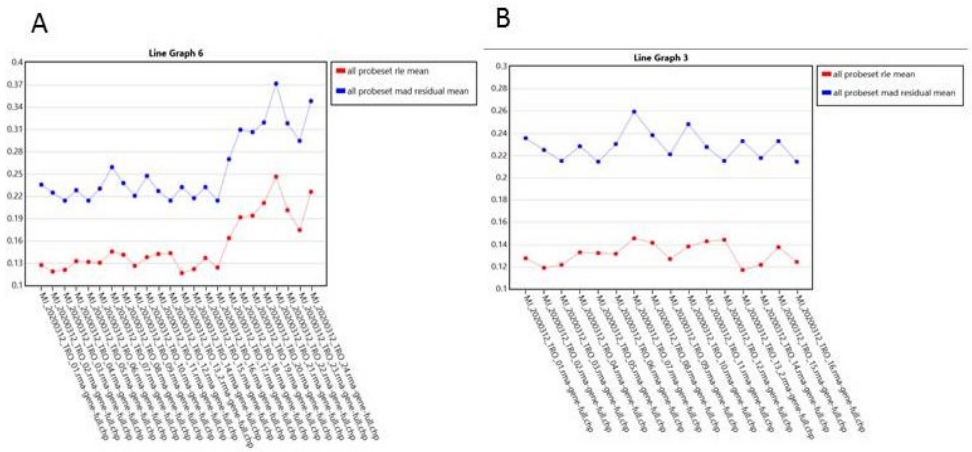

Figure 14 Probeset RLE mean and mad residual mean

The RLE mean considers the signal values for the single probesets compared to the samples of the whole array. High metrics mean a great difference between one sample compared to the rest of the samples. The mad residual mean shows the distinction between the mean and predicted signal value of a sample. Left figure (A) includes outliers and right figure (B) excludes outliers.

6.3.1. Principal component analysis

Principal component analysis provided an overview of similarities and differences in gene expression of the different samples. Each dot represents one object from the respective treatment group. In both PCAs, (with and w/o outliers), samples of "Anti-IFN-γ L7-HA" distinctly clustered together (Figure 15). Wildtypes displayed three outliers, which showed completely different gene expression compared to the other wildtypes (shifted to the right), although the treatment of the animals was exactly the same (Figure 15A). The group L7-HA CD8 showed similarly bad quality parameters as the three WT (Fig 11-14) and were also shifted to the right compared to other groups. Therefore, the three WT and all L7-HA were excluded as their data reliability was too low (Figure 15A). In contrast,

the groups "control IgG" and "IFN-γ-KO" displayed a greater variability within the group in both PCAs, but as the previously analysed parameters revealed a high quality of the data reliability, samples were included in the analyses and variances ascribed to biological differences (Figure 15 A, B). After exclusion of the outliers, quality control was repeated and wildtypes clustered now very well. Anti-IFN-γ showed no striking changes, IFN-γ-KO and conIgG kept their variability (Fig 15B).

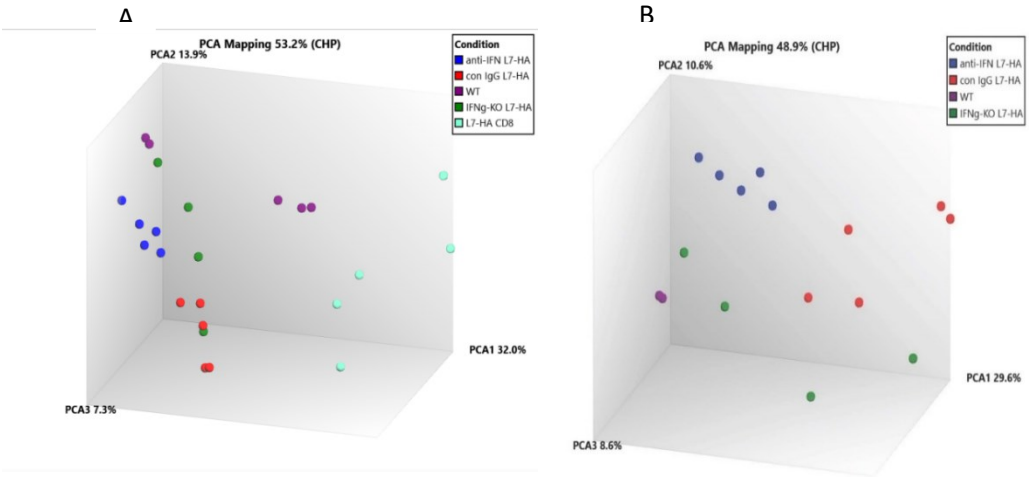

Figure 15 Principal Component Analysis (PCA) w/o outliers

A, B: Group "Anti-IFN-γ" is shown in blue, "WT" is shown in violet, "conIgG" is shown in red and "IFN-γ -KO" is shown in green. Each dot represents one sample.
A: Samples including outliers. L7-HA CD8 is shown in light green. **B:** Samples without outliers.

6.4. Microarray Data Analysis

6.4.1. Gene Set Enrichment Analysis (GSEA)

Enrichment maps were generated on the basis of the differentially expressed genes belonging to distinct pathways in each treatment group. The goal was to determine cell signalling pathways involved in the disease and their role in different biological functions. Furthermore, relations between pathways of different clusters were detected. To achieve this, gene set enrichment analysis was performed and enrichment maps generated.

Enrichment Maps from the comparison of conIgG and WT animals revealed a highly inflammatory and neurodegenerative state

First, groups of conIG and WT were compared. Wildtype animals were supposed to show no pathologic changes and conIgG animals were animals developing PCD accompanied

by strong inflammation, only injected with control immunoglobulins functioning as positive control. Gene set enrichment analysis revealed a downregulation of neuroprotective pathways in conIgGs compared to WTs, contributing to biological functions, such as axon guidance, synaptic transmission and neurotransmitter exocytosis. Compared to WTs, conIgG animals showed an upregulation of proinflammatory pathways involved in antigen processing and presentation via MHCII as well as response to IFN-γ (Figure 16).

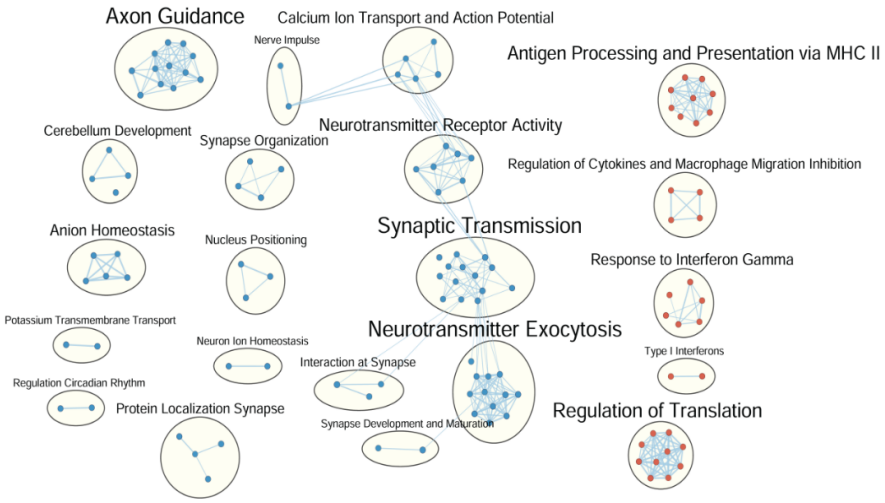

Figure 16 Enrichment Map - conIgG vs. WT

Blue dots indicate pathways downregulated in conIgG compared to WT.
Red dots indicate pathways upregulated in conIgG animals.
The number of nodules (blue or red dots) gives information about the amount of pathways clustering together. One cluster of pathways is marked by a circle and accounts for a special biological function. Lines between circles display similarities between certain pathways that share genes. Line thickness provides information about the amount of genes shared between two connected pathways (The thicker, the more genes are equal in these pathways).

<u>Enrichment Maps from the comparison of conIgG and anti-IFN-γ treated animals revealed a drastically dampened immune response in anti-IFN-γ treated animals.</u>

Next, gene expression of conIgG and anti-IFN-γ was analysed. Compared to conIgG animals, anti-IFN-γ treated animals showed an upregulation of neuroprotective pathways contributing to neuron glial cell signalling and regulation of postsynaptic cytosolic calcium ion concentration. ConIgGs again exhibited upregulated proinflammatory pathways in contrast to anti-IFN-γ animals. These pathways displayed functions in processing and presentation via MHC class II, cytokine signalling and macrophage migration inhibition

(Figure 17).

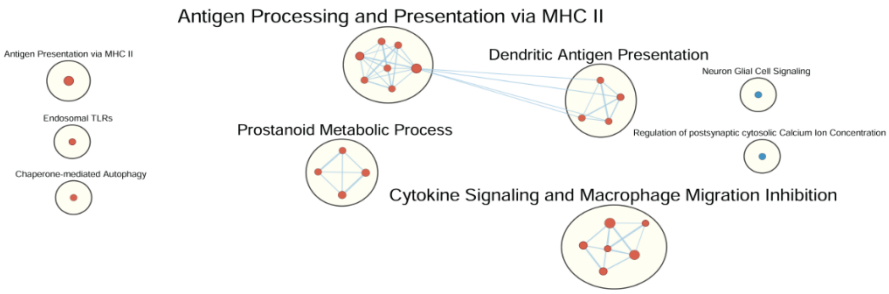

Figure 17 Enrichment Map - conIgG vs. anti-IFN-γ

Red dots represent pathways upregulated in conIgG animals. Blue dots represent pathways upregulated in anti-IFN-γ animals.

Enrichment Maps from the comparison of anti-IFN-γ treated and WT animals revealed no drastic upregulation of inflammatory pathways in anti-IFN-γ animals

Furthermore, WT and anti-IFN-γ were analysed. Wildtypes showed a strong upregulation of pathways involved in respiratory electron transport compared to anti-IFN-γ. Anti-IFN-γ showed an upregulation of pathways participating in neuron homeostasis, regulation of spindle organization and synapse vesicle transport (Figure 18).

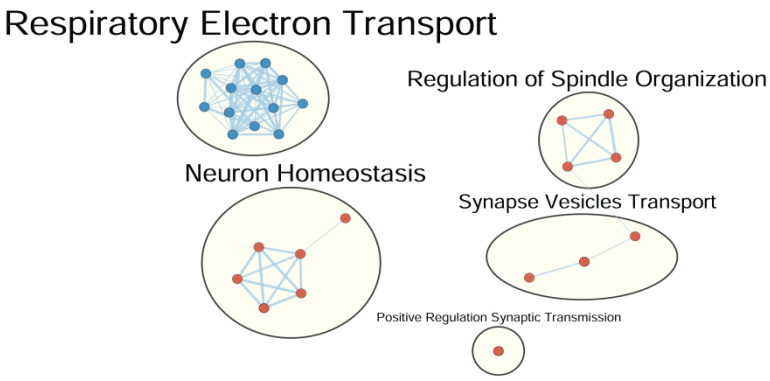

Figure 18 Enrichment Map – Anti-IFN-γ vs. WT

Blue dots indicate an upregulation of pathways in WTs. Red dots indicate an upregulation of pathways in anti-IFN-γ.

7. Discussion

The aim of this thesis was to analyse the cerebellar T cell activity of mice which showed pathology of PCD upon different treatments. For this approach, pathways involved in PCD were examined by transcriptomic gene analysis. Results were supported by histochemical evaluation of T cell numbers in the cerebella of differentially treated groups using light microscopy stainings. Application of confocal laser fluorescence microscope was used to investigate the presence of IFN-γ in correlation with the presence of MHC class I and neuronal loss.

The expression of pro-inflammatory and neuroprotective pathways of each treatment group was demonstrated in gene set enrichment maps and correlated well with the related histological T cell quantifications and confocal microscopy pictures. As expected, wildtypes exhibited an upregulation of pathways contributing to neuronal homeostasis compared to conIgG, which is in line with the absence of T cell mediated neurodegeneration in WT. Confocal microscopy of WTs showed physiological, non-inflammatory conditions indicated by the lack of MHC I upregulation. Moreover, healthy, calbindin rich neurons were present throughout the cerebellum. In contrast, conIgG animals displayed an upregulation of many pro-inflammatory pathways. As expected, pathways participating in IFN-γ response were upregulated in con IgG compared to WTs. The activity of IFN-γ is dependent on signal transducer and activator of transcription 1 (STAT1), which is part of the JAK-STAT signalling pathway. This pathway plays a central role in many cellular processes and can modulate transcription of genes involved many function, e.g. immune cell activation, cell division or regulation of inflammation[106,107].

IFN-γ, uses this signalling pathway to regulate or induce an immune response[108]. Contrary to expectations, pathways involved in antigen processing and presentation via MHC class II molecules were upregulated in conIgG compared to WTs, although CD8 T cell action is associated with MHC class I antigen presentation. The involvement of MHC class II molecules can be explained by the late stage inflammation of the animals in which microglia are activated and express MHC class II molecules on their cell surface.[109] This result correlated with high numbers of T cells infiltrating the cerebellum in conIgG animals and highly activated microglia, shown in the confocal images. Histopathologically, L7-HA CD8 mice showed a similar pattern as the conIgG group. However, due to the bad quality parameters in the microarrays, no information on underlying inflammatory pathways was gained. Moreover, confocal microscopy pictures of conIgG and L7-HA CD8 animals demonstrated a pro-inflammatory environment characterized by high amounts of the markers for pSTAT1 and MHC class I molecules and decreased amounts of calbindin positive cells compared to WTs. These observations underpin previous findings, which show IFN-γ to upregulate MHC class I expression on the surface of neurons to make them more vulnerable to the cytotoxicity of CD8+ T cells[1]. Considering the anti-inflammatory action of anti-IFN-γ in the L7-HA model[1], anti-IFN-γ antibodies were expected to neutralize IFN-γ peripherally in treated animals and to decrease inflammatory events in the cerebellum by decreasing the T cells ability to cross the BBB. Anti-IFN-γ treated animals showed an expression of homeostatic pathways close to physiological levels which, in contrast, was reduced in conIgG. Cell quantifications of anti-IFN-**γ** animals displayed significantly less T cells compared to conIgG and L7-HA CD8 animals. In addition to that, confocal microscopy pictures depicted a lower amount of pSTAT1 positive cells and lower levels of MHC class I upregulation compared to conIgG and L7-HA CD8. Moreover, amounts of calbindin positive cells were closer to physiological levels indicating more healthy neurons than in conIgG and L7-HA CD8. This observation leads to the assumption that anti-IFN-γ treatment could neutralize decisive amounts of IFN-γ and, thus, prevented the consequences of inflammatory reactions promoted by IFN-γ. Anti-IFN-γ animals displayed a healthier, more physiological neuronal environment which was reflected by an upregulation of homeostatic pathways which was not present in conIgG. IFN-γ-KO exhibited great variability in their T cell numbers and pSTAT1 positive cells. These animals received i.p. injections of IFN-γ deficient T cells but no additional

treatment. Therefore, only limiting the onconeural-specific T cell response is not sufficient to decrease neuroinflammation to levels as seen in anti-IFN-γ treated animals. This indicates that other mechanisms, such as bystander T cell activation[110] of endogenous T cells or natural killer[111] cells could have caused the intracerebellar IFN-γ signalling observed in the IFN-γ KO animals.

CD8+ T cells play a central role in the pathology of PCD[1]. As shown in the L7-HA-PCD model, CD8+ T cells infiltrate the cerebellum upon response to hemagglutinin and are found in close proximity to Purkinje cells.[1] Usually, hemagglutinin is a protein expressed in the influenza virus.[112] However, in this model this protein is expressed in genetically engineered cancer cells injected i.p. in the L7-HA model, which in addition, expresses the protein under the promotor L7 in Purkinje neurons of the cerebellum. For this reason, CD8+ T cells specifically target this neuron type during the ICI-promoted immunological overreaction against the tumour, resulting in an autoimmune response[101]. In this inflammatory state, CTLs have been shown to produce harmful amounts of IFN-γ which promotes activation of CTLs. Activated CTLs then attack Purkinje neurons and, thus, induce Purkinje cells death. Due to the central role of CD8+ T cells and IFN-γ on neuronal cell death in PCD[1], this project mainly focussed on these two components.

Upon RNA-quality control, different metric quality parameters of the samples were checked to ensure their suitability for the microarray. Although all samples passed RNA quality controls, microarray quality control revealed in total eight outliers. Three samples of wildtype and five samples of L7-HA CD8 group completely differed in their parameters from the other samples. Although, all wildtypes showed absence of T cell infiltrations in the cerebellum and were treated equally, sample behaviour of three wildtypes differed from the remaining wildtypes as observed in the PCA plot. The outliers´ shifted positions in the plot could be based on deficient RNA quality due to the fixation method of the tissue which causes many modulations in the RNA, such as breaks in the sugar-phosphate backbone of nucleic acids[102]. Furthermore, also post-mortem delay and prolonged fixation times could have contributed to deficient RNA quality[102]. Also, it is known, that these eight outliers origin from a different batch than the other samples and, therefore, different sample handling could have caused the completely different sample behaviour.

Moreover, IFN-γ-KO group passed all quality controls, however showed a great variety in gene expression within the group and was, hence, also excluded from GSEA.

To sum up, this project further underlines the great potential of anti-IFN-γ antibodies in the treatment of PCD and emphasizes IFN-γ as an important mediator in inflammation and recruitment of immune cells. Further investigative approaches could imply L7-HA PCD animals at different disease stages with and without the influence of anti-IFN-γ to better understand the interplay of CD8 T cells with other immune components, but also to get more insight into the progress of PCD.

8. Abbrevations

%	Percent
a.d.	Aqua destillata
Ab	Antibody
AMPA	Alpha-amino-3-hydroxy-5-methyl-4-isoxazdepropionic acid
ANNA-1	Type1 anti-neuronal nuclear antibody
ANNA-2	Type2 anti-neuronal nuclear antibody
APC	Antigen-presenting cells
AUC	Area under the curve
BBB	Blood-Brain barrier
BCSFB	Blood-cerebrospinal fluid barrier
Bgrd	Background
CD	Cluster of Differentiation
cDNA	Complementary DNA
CDR2	Cerebellar degeneration-related antigen
CNS	Central nervous system
Con	Control
CSA	Catalysed signal amplification system
CSF	Cerebrospinal fluid
CTL	Cytotoxic T cell
CTLA-4	Cytotoxic Lymphocyte Antigen-4
DAB	3,3´- Diaminobenzen
DAMPS	Damage-associated molecular patterns
DC	Dendritic cells
DV	Distribution Value
EC	Endothelial cell
EDTA	Ethylenediaminetetraacetic acid

EtOH	Ethanol
FCS	Fetal calf serum
FFPE	Formalin fixed, paraffin-embedded
G	Gram
gDNA	Genomic deoxyribonucleic acid
HA	Hemagglutinin
IC	Immune checkpoint
ICI	Immune checkpoint inhibitor
IFN-γ	Interferon gamma
Ig	Immunglobuline
IL	Interleukin
i.p.	Intraperitoneal
IrAE	Immune-related adverse events
KO	Knock-out
MHC	Major histocompatibility complex
ml	Milliliters
mM	Millimolar
nirAE	Neurological immune-related adverse events
NMDA	Anti-N-methyl-D-aspartate
PBS	Phosphate-Buffered Saline
PCA	Principal component analysis
PCA-1	Purkinje cell cytoplasmic antibody
PCD	Paraneoplastic cerebellar degeneration
PD-1	Programmed Death-1 antibody
pH	Potential hydrogen
PNA	Paraneoplastic neuronal autoantibodies
PNS	Paraneoplastic neurological syndrome

PRR	Pattern recognition receptor
Pstat	Phosphorylated Signal Transducers and Activators of Transcription
qPCR	Quantitative Polymerase Chain Reaction
Rle	Relative log expression
RT	Reverse Transcription
SCLC	Small Cell Lung Cancer
SDS	Sodium dodecyl sulfate
TBS	Tris buffered saline
TCR	T cell receptor
Th	T helper
TLR	Toll-like receptor
WT	Wildtype

9. Literature

1. Yshii L, Pignolet B, Mauré E, et al. IFN-γ is a therapeutic target in paraneoplastic cerebellar degeneration. *JCI Insight*. Published online 2019. doi:10.1172/jci.insight.127001

2. Graus F, Dalmau J. Paraneoplastic neurological syndromes in the era of immune-checkpoint inhibitors. *Nat Rev Clin Oncol*. Published online 2019. doi:10.1038/s41571-019-0194-4

3. Vogrig A, Muñiz-Castrillo S, Desestret V, Joubert B, Honnorat J. Pathophysiology of paraneoplastic and autoimmune encephalitis: genes, infections, and checkpoint inhibitors. *Ther Adv Neurol Disord*. Published online 2020. doi:10.1177/1756286420932797

4. Leypoldt F, Wandinger KP. Paraneoplastic neurological syndromes. *Clin Exp Immunol*. Published online 2014. doi:10.1111/cei.12185

5. Honnorat J, Antoine JC. Paraneoplastic neurological syndromes. *Orphanet J Rare Dis*. Published online 2007. doi:10.1186/1750-1172-2-22

6. Ardolino L, Joshua A. Immune checkpoint inhibitors in malignancy. *Aust Prescr*. Published online 2019. doi:10.18773/austprescr.2019.012

7. Le May M, Dent S. Anti-yo antibody–mediated paraneoplastic cerebellar degeneration associated with cognitive affective syndrome in a patient with breast cancer: A case report and literature review. *Curr Oncol*. Published online 2018. doi:10.3747/co.25.4106

8. Freire MO, Van Dyke TE. Natural resolution of inflammation. *Periodontol 2000*. Published online 2013. doi:10.1111/prd.12034

9. Lucas SM, Rothwell NJ, Gibson RM. The role of inflammation in CNS injury and disease. *Br J Pharmacol*. Published online 2006. doi:10.1038/sj.bjp.0706400

10. Carson MJ, Doose JM, Melchior B, Schmid CD, Ploix CC. CNS immune privilege: Hiding in plain sight. *Immunol Rev*. Published online 2006. doi:10.1111/j.1600-065X.2006.00441.x

11. Duan L, Rao X, Sigdel KR. Regulation of inflammation in autoimmune disease. *J Immunol Res*. Published online 2019. doi:10.1155/2019/7403796

12. MEDAWAR PB. Immunity to homologous grafted skin; the relationship between the antigens of blood and skin. *Br J Exp Pathol*. Published online 1946.

13. Forrester J V., McMenamin PG, Dando SJ. CNS infection and immune privilege. *Nat Rev Neurosci*. Published online 2018. doi:10.1038/s41583-018-0070-8

14. Park HS, Park MJ, Kwon MS. Central nervous system-peripheral immune system dialogue in neurological disorders: Possible application of neuroimmunology in

urology. *Int Neurourol J*. Published online 2016. doi:10.5213/inj.1632614.307

15. Huber AK, Irani DN. Is the concept of central nervous system immune privilege irrelevant in the setting of acute infection? *Front Oncol*. Published online 2015. doi:10.3389/fonc.2015.00099

16. Małkiewicz MA, Szarmach A, Sabisz A, Cubała WJ, Szurowska E, Winklewski PJ. Blood-brain barrier permeability and physical exercise. *J Neuroinflammation*. Published online 2019. doi:10.1186/s12974-019-1403-x

17. Shastri A, Bonifati DM, Kishore U. Innate immunity and neuroinflammation. *Mediators Inflamm*. Published online 2013. doi:10.1155/2013/342931

18. Moore CS, Durafourt BA, Antel JP. Innate Immunity in the CNS - A Focus on the Myeloid Cell. In: *Neuroinflammation and CNS Disorders*. ; 2014. doi:10.1002/9781118406557.ch2

19. Carrillo JLM, Rodríguez FPC, Coronado OG, García MAM, Cordero JFC. Physiology and Pathology of Innate Immune Response Against Pathogens. In: *Physiology and Pathology of Immunology*. ; 2017. doi:10.5772/intechopen.70556

20. Hato T, Dagher PC. How the innate immune system senses trouble and causes trouble. *Clin J Am Soc Nephrol*. Published online 2015. doi:10.2215/CJN.04680514

21. Aristizábal B GÁ. Autoimmunity: From Bench to Bedside. In: Anaya JM, Shoenfeld Y, Rojas-Villarraga A, A Levy RC, ed. *Autoimmunity: From Bench to Bedside*. first Edit. El Rosario University Press; 2013. https://www.ncbi.nlm.nih.gov/books/NBK459455/

22. Théry C, Amigorena S. The cell biology of antigen presentation in dendritic cells. *Curr Opin Immunol*. Published online 2001. doi:10.1016/S0952-7915(00)00180-1

23. Janeway CA Jr, Travers P WM. *Principles of Innate and Adaptive Immunity*. 5th ed. (Penelope Austin EL, ed.). Garland Publishing; 2001. https://www.ncbi.nlm.nih.gov/books/NBK27090/

24. Ndubaku U, de Bellard ME. Glial cells: Old cells with new twists. *Acta Histochem*. Published online 2008. doi:10.1016/j.acthis.2007.10.003

25. Rasband MN. Glial contributions to neural function and disease. *Mol Cell Proteomics*. Published online 2016. doi:10.1074/mcp.R115.053744

26. Nayak D, Roth TL, McGavern DB. Microglia Development and Function. *Annu Rev Immunol*. Published online 2014. doi:10.1146/annurev-immunol-032713-120240

27. Xavier AL, Menezes JRL, Goldman SA, Nedergaard M. Fine-tuning the central nervous system: Microglial modelling of cells and synapses. *Philos Trans R Soc B Biol Sci*. Published online 2014. doi:10.1098/rstb.2013.0593

28. Rock RB, Gekker G, Hu S, et al. Role of microglia in central nervous system infections. *Clin Microbiol Rev*. Published online 2004. doi:10.1128/CMR.17.4.942-

964.2004

29. Colonna M, Butovsky O. Microglia Function in the Central Nervous System During Health and Neurodegeneration. *Annu Rev Immunol*. Published online 2017. doi:10.1146/annurev-immunol-051116-052358

30. Kierdorf K, Prinz M. Factors regulating microglia activation. *Front Cell Neurosci*. Published online 2013. doi:10.3389/fncel.2013.00044

31. Herculano-Houzel S. The glia/neuron ratio: How it varies uniformly across brain structures and species and what that means for brain physiology and evolution. *Glia*. Published online 2014. doi:10.1002/glia.22683

32. Leung AW, Li JYH. The Molecular Pathway Regulating Bergmann Glia and Folia Generation in the Cerebellum. *Cerebellum*. Published online 2018. doi:10.1007/s12311-017-0904-3

33. Matyash V, Kettenmann H. Heterogeneity in astrocyte morphology and physiology. *Brain Res Rev*. Published online 2010. doi:10.1016/j.brainresrev.2009.12.001

34. Nutma E, van Gent D, Amor S, Peferoen LAN. Astrocyte and Oligodendrocyte Cross-Talk in the Central Nervous System. *Cells*. Published online 2020. doi:10.3390/cells9030600

35. Colombo E, Farina C. Astrocytes: Key Regulators of Neuroinflammation. *Trends Immunol*. Published online 2016. doi:10.1016/j.it.2016.06.006

36. Daneman R, Prat A. The blood–brain barrier. *Cold Spring Harb Perspect Biol*. Published online 2015. doi:10.1101/cshperspect.a020412

37. Xu L, Nirwane A, Yao Y. Basement membrane and blood-brain barrier. *Stroke Vasc Neurol*. Published online 2019. doi:10.1136/svn-2018-000198

38. Attwell D, Mishra A, Hall CN, O'Farrell FM, Dalkara T. What is a pericyte? *J Cereb Blood Flow Metab*. Published online 2016. doi:10.1177/0271678X15610340

39. Kubotera H, Ikeshima-Kataoka H, Hatashita Y, Allegra Mascaro AL, Pavone FS, Inoue T. Astrocytic endfeet re-cover blood vessels after removal by laser ablation. *Sci Rep*. Published online 2019. doi:10.1038/s41598-018-37419-4

40. Janzer RC, Raff MC. Astrocytes induce blood-brain barrier properties in endothelial cells. *Nature*. Published online 1987. doi:10.1038/325253a0

41. Netto JP, Iliff J, Stanimirovic D, et al. Neurovascular unit: Basic and clinical imaging with emphasis on advantages of ferumoxytol. *Neurosurgery*. Published online 2018. doi:10.1093/neuros/nyx357

42. Yu X, Ji C, Shao A. Neurovascular Unit Dysfunction and Neurodegenerative Disorders. *Front Neurosci*. Published online 2020. doi:10.3389/fnins.2020.00334

43. Varatharaj A, Galea I. The blood-brain barrier in systemic inflammation. *Brain*

Behav Immun. Published online 2017. doi:10.1016/j.bbi.2016.03.010

44. Marshall JS, Warrington R, Watson W, Kim HL. An introduction to immunology and immunopathology. *Allergy, Asthma Clin Immunol*. Published online 2018. doi:10.1186/s13223-018-0278-1

45. Neurath AR. Immune Response to Viruses: Antibody-Mediated Immunity. In: *Encyclopedia of Virology*. ; 2008:56-70. doi:10.1016/B978-012374410-4.00591-4

46. Berard M, Tough DF. Qualitative differences between naïve and memory T cells. *Immunology*. Published online 2002. doi:10.1046/j.1365-2567.2002.01447.x

47. Luckheeram RV, Zhou R, Verma AD, Xia B. CD4 +T cells: Differentiation and functions. *Clin Dev Immunol*. Published online 2012. doi:10.1155/2012/925135

48. Gebauer C. The Janus face of immunity: how anti-tumor immunity leads to autoimmunity in paraneoplastic neurological diseases. Published online 2017. https://tel.archives-ouvertes.fr/tel-01492922/file/2016TOU30139b.pdf

49. Pennock ND, White JT, Cross EW, Cheney EE, Tamburini BA, Kedl RM. T cell responses: Naïve to memory and everything in between. *Am J Physiol - Adv Physiol Educ*. Published online 2013. doi:10.1152/advan.00066.2013

50. Sarkar S, Horn G, Moulton K, et al. Cancer development, progression, and therapy: An epigenetic overview. *Int J Mol Sci*. Published online 2013. doi:10.3390/ijms141021087

51. Cooper JP, Youle RJ. Balancing cell growth and death. *Curr Opin Cell Biol*. Published online 2012. doi:10.1016/j.ceb.2012.11.003

52. Barnum KJ, O'Connell MJ. Cell cycle regulation by checkpoints. *Methods Mol Biol*. Published online 2014. doi:10.1007/978-1-4939-888-2_2

53. Centelles JJ. General Aspects of Colorectal Cancer. *ISRN Oncol*. Published online 2012. doi:10.5402/2012/139268

54. Organization WH. Cancer prevention. Accessed July 2, 2020. https://www.who.int/cancer/prevention/en/

55. Rakoff-Nahoum S. Why cancer and inflammation? *Yale J Biol Med*. Published online 2006.

56. Gonzalez S, González-Rodríguez AP, Suárez-Álvarez B, López-Soto A, Huergo-Zapico L, Lopez-Larrea C. Conceptual aspects of self and nonself discrimination. *Self/Nonself - Immune Recognit Signal*. Published online 2011. doi:10.4161/self.2.1.15094

57. Pandya PH, Murray ME, Pollok KE, Renbarger JL. The Immune System in Cancer Pathogenesis: Potential Therapeutic Approaches. *J Immunol Res*. Published online 2016. doi:10.1155/2016/4273943

58. Dunn GP, Bruce AT, Ikeda H, Old LJ, Schreiber RD. Cancer immunoediting: From

immunosurveillance to tumor escape. *Nat Immunol*. Published online 2002. doi:10.1038/ni1102-991

59. Nishida N, Yano H, Nishida T, Kamura T, Kojiro M. Angiogenesis in cancer. *Vasc Health Risk Manag*. Published online 2006. doi:10.2147/vhrm.2006.2.3.213

60. Finn OJ. Immuno-oncology: Understanding the function and dysfunction of the immune system in cancer. In: *Annals of Oncology*. ; 2012. doi:10.1093/annonc/mds256

61. Mittal D, Gubin MM, Schreiber RD, Smyth MJ. New insights into cancer immunoediting and its three component phases-elimination, equilibrium and escape. *Curr Opin Immunol*. Published online 2014. doi:10.1016/j.coi.2014.01.004

62. Mellman I, Coukos G, Dranoff G. Cancer immunotherapy comes of age. *Nature*. Published online 2011. doi:10.1038/nature10673

63. Nirschl CJ, Drake CG. Molecular pathways: Coexpression of immune checkpoint molecules: Signaling pathways and implications for cancer immunotherapy. *Clin Cancer Res*. Published online 2013. doi:10.1158/1078-0432.CCR-12-1972

64. Sperk M, van Domselaar R, Neogi U. Immune checkpoints as the immune system regulators and potential biomarkers in HIV-1 infection. *Int J Mol Sci*. Published online 2018. doi:10.3390/ijms19072000

65. Sansom DM. CD28, CTLA-4 and their ligands: Who does what and to whom? *Immunology*. Published online 2000. doi:10.1046/j.1365-2567.2000.00121.x

66. Buchbinder EI, Desai A. CTLA-4 and PD-1 Pathways. *Am J Clin Oncol*. Published online 2016. doi:10.1097/coc.0000000000000239

67. Rotte A, Jin JY, Lemaire V. Mechanistic overview of immune checkpoints to support the rational design of their combinations in cancer immunotherapy. *Ann Oncol*. Published online 2018. doi:10.1093/annonc/mdx686

68. Krummel MF, Allison JP. CD28 and CTLA-4 have opposing effects on the response of T ceils to stimulation. *J Exp Med*. Published online 1995. doi:10.1084/jem.182.2.459

69. Takahashi T, Tagami T, Yamazaki S, et al. Immunologic self-tolerance maintained by CD25+CD4+ regulatory T cells constitutively expressing cytotoxic T lymphocyte-associated antigen 4. *J Exp Med*. Published online 2000. doi:10.1084/jem.192.2.303

70. Wing K, Onishi Y, Prieto-Martin P, et al. CTLA-4 control over Foxp3+ regulatory T cell function. *Science (80-)*. Published online 2008. doi:10.1126/science.1160062

71. Pardoll DM. The blockade of immune checkpoints in cancer immunotherapy. *Nat Rev Cancer*. Published online 2012. doi:10.1038/nrc3239

72. Sharpe AH. Introduction to checkpoint inhibitors and cancer immunotherapy.

Immunol Rev. Published online 2017. doi:10.1111/imr.12531

73. Rausch MP, Hastings KT. Immune Checkpoint Inhibitors in the Treatment of Melanoma: From Basic Science to Clinical Application. In: *Cutaneous Melanoma: Etiology and Therapy*. ; 2017. doi:10.15586/codon.cutaneousmelanoma.2017.ch9

74. Postow M a., Wolchok JD. Toxicities associated with checkpoint inhibitor immunotherapy. *UpToDate*. Published online 2016.

75. Seidel JA, Otsuka A, Kabashima K. Anti-PD-1 and anti-CTLA-4 therapies in cancer: Mechanisms of action, efficacy, and limitations. *Front Oncol*. Published online 2018. doi:10.3389/fonc.2018.00086

76. Bajwa R, Cheema A, Khan T, et al. Adverse Effects of Immune Checkpoint Inhibitors (Programmed Death-1 Inhibitors and Cytotoxic T-Lymphocyte-Associated Protein-4 Inhibitors): Results of a Retrospective Study. *J Clin Med Res*. Published online 2019. doi:10.14740/jocmr3750

77. Spiers L, Coupe N, Payne M. Toxicities associated with checkpoint inhibitors-An overview. *Rheumatol (United Kingdom)*. Published online 2019. doi:10.1093/rheumatology/kez418

78. Möhn N, Beutel G, Gutzmer R, Ivanyi P, Satzger I, Skripu T. Neurological Immune Related Adverse Events Associated with Nivolumab, Ipilimumab, and Pembrolizumab Therapy—Review of the Literature and Future Outlook. *J Clin Med*. Published online 2019. doi:10.3390/jcm8111777

79. Ramos-Casals M, Brahmer JR, Callahan MK, et al. Immune-related adverse events of checkpoint inhibitors. *Nat Rev Dis Prim*. Published online 2020. doi:10.1038/s41572-020-0160-6

80. Darnell RB, Posner JB. Paraneoplastic syndromes involving the nervous system. *N Engl J Med*. Published online 2003. doi:10.1056/NEJMra023009

81. Dalmau J, Gultekin HS, Posner JB. Paraneoplastic Neurologic Syndromes: Pathogenesis and Physiopathology. *Brain Pathol*. Published online 2006. doi:10.1111/j.1750-3639.1999.tb00226.x

82. Dalmau J, Geis C, Graus F. Autoantibodies to synaptic receptors and neuronal cell surface proteins in autoimmune diseases of the central nervous system. *Physiol Rev*. Published online 2017. doi:10.1152/PHYSREV.00010.2016

83. Susumu Kusunoki. Paraneoplastic Neurological Syndrome. In: Kusunoki S, ed. *Neuroimmunological Diseases*. Springer Japan; 2016:292. doi:10.1007/978-4-431-55594-0

84. Kannoth S. Paraneoplastic neurologic syndrome: A practical approach. *Ann Indian Acad Neurol*. Published online 2012. doi:10.4103/0972-2327.93267

85. Gebauer C, Pignolet B, Yshii L, Mauré E, Bauer J, Liblau R. CD4+ and CD8+ T cells are both needed to induce paraneoplastic neurological disease in a mouse

model. *Oncoimmunology*. Published online 2017. doi:10.1080/2162402X.2016.1260212

86. Rojas I, Graus F, Keime-Guibert F, et al. Long-term clinical outcome of paraneoplastic cerebellar degeneration and anti-Yo antibodies. *Neurology*. Published online 2000. doi:10.1212/WNL.55.5.713

87. Hammack J, Kotanides H, Rosenblum MK, Posner JB. Paraneoplastic cerebellar degeneration: II. clinical and immunologic findings in 21 patients with hodgkin's disease. *Neurology*. Published online 1992. doi:10.1212/wnl.42.10.1938

88. Dalmau J, Rosenfeld MR. Paraneoplastic syndromes of the CNS. *Lancet Neurol*. Published online 2008. doi:10.1016/S1474-4422(08)70060-7

89. Greenfield JG. Subacute spino-cerebellar degeneration occurring in elderly patients. *Brain*. Published online 1934. doi:10.1093/brain/57.2.161

90. Darnell JC, Albert ML, Darnell RB. cdr2, A target antigen of naturally occurring human tumor immunity, is widely expressed in gynecological tumors. *Cancer Res*. Published online 2000.

91. Giometto B, Marchiori GC, Nicolao P, et al. Sub-acute cerebellar degeneration with anti-Yo autoantibodies: Immunohistochemical analysis of the immune reaction in the central nervous system. *Neuropathol Appl Neurobiol*. Published online 1997. doi:10.1111/j.1365-2990.1997.tb01323.x

92. BRAIN WR, DANIEL PM, GREENFIELD JG. Subacute cortical cerebellar degeneration and its relation to carcinoma. *J Neurol Neurosurg Psychiatry*. Published online 1951. doi:10.1136/jnnp.14.2.59

93. Brock S, Illidge T, Ellison D, Frankel J, Davis C. Anti-yo antibody-positve cerebellar degeneration associated with endometrial carcinoma: Case report and review of the literature. *Clin Oncol*. Published online 2001. doi:10.1053/clon.2001.9318

94. Spencer KA, Slocomb DL. The neural basis of ataxic dysarthria. *Cerebellum*. Published online 2007. doi:10.1080/14734220601145459

95. Alves M, Miranda A, Narciso MR, Mieiro L, Fonseca T. Diplopia: A diagnostic challenge with common and rare etiologies. *Am J Case Rep*. Published online 2015. doi:10.12659/AJCR.893134

96. Peterson K, Rosenblum MK, Kotanides H, Posner JB. Paraneoplastic cerebellar degeneration: I.A clinical analysis of 55 anti–Yo antibody–positive patients. *Neurology*. Published online 1992. doi:10.1212/wnl.42.10.1931

97. Shams'Ili S, Grefkens J, De Leeuw B, et al. Paraneoplastic cerebellar degeneration associated with antineuronal antibodies: Analysis of 50 patients. *Brain*. Published online 2003. doi:10.1093/brain/awg133

98. Paslawski T, Duffy JR, Vernino S. Speech and language findings associated with paraneoplastic cerebellar degeneration. *Am J Speech-Language Pathol*. Published

online 2005. doi:10.1044/1058-0360(2005/020)

99. Rees JH. Paraneoplastic syndromes: When to suspect, how to confirm, and how to manage. *Neurol Pract*. Published online 2004. doi:10.1136/jnnp.2004.040378

100. Candler PM, Hart PE, Barnett M, Weil R, Rees JH. A follow up study of patients with paraneoplastic neurological disease in the United Kingdom. *J Neurol Neurosurg Psychiatry*. Published online 2004. doi:10.1136/jnnp.2003.025171

101. Yshii LM, Gebauer CM, Pignolet B, et al. CTLA4 blockade elicits paraneoplastic neurological disease in a mouse model. *Brain*. Published online 2016. doi:10.1093/brain/aww225

102. Wimmer I, Tröscher AR, Brunner F, et al. Systematic evaluation of RNA quality, microarray data reliability and pathway analysis in fresh, fresh frozen and formalin-fixed paraffin-embedded tissue samples. *Sci Rep*. Published online 2018. doi:10.1038/s41598-018-24781-6

103. Raudvere U, Kolberg L, Kuzmin I, et al. G:Profiler: A web server for functional enrichment analysis and conversions of gene lists (2019 update). *Nucleic Acids Res*. Published online 2019. doi:10.1093/nar/gkz369

104. Bien CG, Bauer J. T-cells in human encephalitis. *NeuroMolecular Med*. Published online 2005. doi:10.1385/NMM:7:3:243

105. Puntel M, Barrett R, Sanderson NSR, et al. Identification and visualization of CD8 + T cell mediated IFN-γ signaling in target cells during an antiviral immune response in the brain. *PLoS One*. Published online 2011. doi:10.1371/journal.pone.0023523

106. Rawlings JS, Rosler KM, Harrison DA. The JAK/STAT signaling pathway. *J Cell Sci*. Published online 2004. doi:10.1242/jcs.00963

107. Hu X, Ivashkiv LB. Cross-regulation of Signaling Pathways by Interferon-γ: Implications for Immune Responses and Autoimmune Diseases. *Immunity*. Published online 2009. doi:10.1016/j.immuni.2009.09.002

108. Owen KL, Brockwell NK, Parker BS. Jak-stat signaling: A double-edged sword of immune regulation and cancer progression. *Cancers (Basel)*. Published online 2019. doi:10.3390/cancers11122002

109. Schetters STT, Gomez-Nicola D, Garcia-Vallejo JJ, Van Kooyk Y. Neuroinflammation: Microglia and T cells get ready to tango. *Front Immunol*. Published online 2018. doi:10.3389/fimmu.2017.01905

110. Kim TS, Shin EC. The activation of bystander CD8+ T cells and their roles in viral infection. *Exp Mol Med*. Published online 2019. doi:10.1038/s12276-019-0316-1

111. Mah AY, Cooper MA. Metabolic regulation of natural killer cell IFN-γ production. *Crit Rev Immunol*. Published online 2016. doi:10.1615/CritRevImmunol.2016017387

112. Sriwilaijaroen N, Suzuki Y. Molecular basis of the structure and function of H1 hemagglutinin of influenza virus. *Proc Japan Acad Ser B Phys Biol Sci*. Published online 2012. doi:10.2183/pjab.88.226